Article

Cell

Sensory Neurons that Detect Stretch and Nutrients in the Digestive System

Graphical Abstract

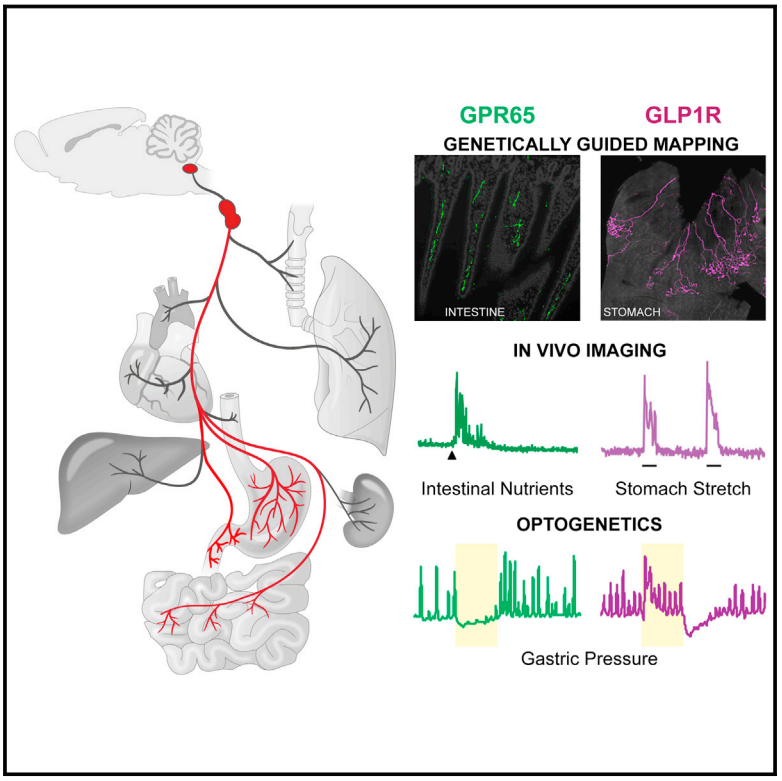

Authors

Erika K. Williams, Rui B. Chang, David E. Strochlic, Benjamin D. Umans, Bradford B. Lowell, Stephen D. Liberles

Correspondence

stephen_liberles@hms.harvard.edu

In Brief

Two types of neurons sending signals from the gut to the brain control digestion. One densely innervates intestinal villi and detects food, while another targets stomach and intestinal muscle and senses stretch.

Highlights

- Genetic deconstruction of vagal afferent types that monitor and control digestion
- GPR65 neurons target intestinal villi, detect nutrients, and control gut motility
- GLP1R neurons form specialized terminals that detect stomach and intestine stretch
- Coding of autonomic inputs in vagal ganglion and brainstem

Williams et al., 2016, Cell *166*, 209–221
June 30, 2016 © 2016 Elsevier Inc.
http://dx.doi.org/10.1016/j.cell.2016.05.011

CellPress

Article

Cell

Sensory Neurons that Detect Stretch and Nutrients in the Digestive System

Erika K. Williams,[1,3] Rui B. Chang,[1,3] David E. Strochlic,[1,3] Benjamin D. Umans,[1] Bradford B. Lowell,[2] and Stephen D. Liberles[1,*]

[1]Department of Cell Biology, Harvard Medical School, Boston, MA 02115, USA

[2]Division of Endocrinology, Diabetes and Metabolism, Department of Medicine, Beth Israel Deaconess Medical Center, Harvard Medical School, Boston, MA 02115, USA

[3]Co-first author

*Correspondence: stephen_liberles@hms.harvard.edu

http://dx.doi.org/10.1016/j.cell.2016.05.011

SUMMARY

Neural inputs from internal organs are essential for normal autonomic function. The vagus nerve is a key body-brain connection that monitors the digestive, cardiovascular, and respiratory systems. Within the gastrointestinal tract, vagal sensory neurons detect gut hormones and organ distension. Here, we investigate the molecular diversity of vagal sensory neurons and their roles in sensing gastrointestinal inputs. Genetic approaches allowed targeted investigation of gut-to-brain afferents involved in homeostatic responses to ingested nutrients (GPR65 neurons) and mechanical distension of the stomach and intestine (GLP1R neurons). Optogenetics, in vivo ganglion imaging, and genetically guided anatomical mapping provide direct links between neuron identity, peripheral anatomy, central anatomy, conduction velocity, response properties in vitro and in vivo, and physiological function. These studies clarify the roles of vagal afferents in mediating particular gut hormone responses. Moreover, genetic control over gut-to-brain neurons provides a molecular framework for understanding neural control of gastrointestinal physiology.

INTRODUCTION

In addition to our external senses of sight, smell, sound, touch, and taste, internal sensory systems within our body relay vital information to the brain about physiological state. The vagus nerve is a major information highway from the periphery that innervates, surveys, and controls several principal physiological systems. Within the gastrointestinal tract, vagal sensory neurons monitor stomach volume and intestinal contents, and responsive neural circuits regulate digestive physiology (Brookes et al., 2013). However, a molecular and genetic classification of gastrointestinal fibers within the vagus nerve is not available and would facilitate mechanistic studies of gut-to-brain signaling in health and disease.

The mouse vagus nerve contains ~2,300 sensory neurons with cell bodies in ganglia at the base of the skull, as well as a smaller group of motor neurons with soma in the brainstem. Each sensory neuron has both a peripheral terminal that interfaces with an internal organ and a central brainstem terminal. Classical anatomical tracing studies revealed a variety of terminal types within the gastrointestinal tract (Berthoud et al., 2004). Stomach terminals include mucosal endings, intraganglionic laminar endings (IGLEs), and intramuscular arrays. Gastric IGLEs contact enteric ganglia between layers of stomach muscle (Fox et al., 2000) and are proposed to sense stomach stretch, as they are near sites of mechanosensation (Zagorodnyuk et al., 2001). In the intestine, vagal afferents form IGLEs, endings near intestinal crypts, and free terminals embedded within the lamina propria of intestinal villi (Berthoud et al., 2004).

Vagal afferents have been proposed to detect nutrients at several locations, including in proximal and distal intestine and the hepatic portal system (Maljaars et al., 2008; Rüttimann et al., 2009). Because vagal afferents do not directly contact the intestinal lumen, vagal nutrient detectors are likely to be second-order chemosensory neurons. Terminals in intestinal villi are excellent candidates to contribute to nutrient detection; however, specific characterization of sensory neurons with villous terminals has been technically challenging. Lumen-proximal endings were defined in some studies by sensitivity to mucosal stroking or luminal anesthetics (Blackshaw and Grundy, 1990; Richards et al., 1996); however, these manipulations may not selectively impact all villous terminals. Additional insights could be provided by genetically defining nutrient-responsive vagal afferents and subsequently examining their terminal fields in the periphery.

Different models have been raised for how the vagus nerve receives and encodes information about ingested nutrients. Some studies reported polymodal responses of single vagal afferents to intestinal nutrients, as well as to changes in osmolarity and pH (Mei and Garnier, 1986; Zhu et al., 2001). Other studies concluded that vagal afferents are highly tuned for specific nutrients, with different fibers dedicated for sugars, amino acids, and fats (Jeanningros, 1982; Lal et al., 2001; Mei, 1978). Ingested nutrients activate enteroendocrine cells, sparsely distributed sentinel cells in the intestinal epithelium. Enteroendocrine cells respond to nutrients by releasing a myriad of gut hormones, including serotonin, glucagon-like peptide 1 (GLP1), cholecystokinin (CCK), peptide

YY, and others (Chambers et al., 2013). Detection of different nutrients, perhaps through taste receptors (Jang et al., 2007), may evoke differential hormone secretion. Release of serotonin by enterochromaffin cells has also been linked to nausea-inducing toxins, inflammatory cues, mechanical forces, and commensal microflora (Bertrand and Bertrand, 2010; Yano et al., 2015). Once released, gut hormones orchestrate powerful systemic responses to nutrient intake and can act locally as paracrine signals and distally after entering circulation. Vagus nerve terminals in intestinal villi occupy a privileged anatomical location to detect gut hormones.

Basic questions remain about the extent of functional overlap between different gut hormones and whether they encode specific or redundant messages about intestinal stimuli to the vagus nerve. Perhaps best studied are serotonin and cholecystokinin, which activate different vagal afferents (Hillsley and Grundy, 1998). In some electrophysiological studies, each of these gut hormones reportedly activates lumen-proximal or nutrient-responsive vagal afferents (Blackshaw and Grundy, 1990; Zhu et al., 2001). In other studies, the same gut hormones reportedly activate mechanoreceptors (Mazda et al., 2004; Schwartz et al., 1991). Different studies also claimed important roles for each hormone in various nutrient-evoked physiological responses (Chambers et al., 2013). A limitation of in vivo pharmacology is that injection of CCK or serotonin causes indirect responses, such as changes in gastrointestinal motility and tone. Genetic tools that enable selective labeling of villous-projecting neurons would enable precise characterization of gut hormone responsiveness in vitro.

GLP1 is another gut hormone proposed to mediate aspects of nutrient detection by the vagus nerve (Holst, 2007). Incretin therapies that involve mimicry or stabilization of GLP1 provide an important strategy for treatment of metabolic disease. GLP1 is detected by a dedicated G protein-coupled receptor (GLP1R) expressed in many cell types (Thorens, 1992). Studies involving localized injection of GLP1R agonists have concluded important roles for GLP1 reception in various locations, including the brain and periphery (Hayes et al., 2010). Some vagal afferents express GLP1R, and some vagal afferents are positioned within intestinal villi near enteroendocrine cells. It has been presumed that these are the same sensory neurons, and as such, it has been proposed that GLP1R contributes to vagal detection of intestinal nutrients. Surgical vagotomy reportedly impairs GLP1-evoked physiological responses in some studies but not others (Abbott et al., 2005; Zhang and Ritter, 2012), and effects could be due to loss of sensory or motor neurons. However, genetic deletion of GLP1R from PHOX2B-expressing vagal afferents does not impact GLP1R agonist-induced changes in body weight and glucose homeostasis (Sisley et al., 2014). Taken together, basic questions persist about the anatomy, responses, and functions of vagal GLP1R neurons.

Here, we used genetic approaches to study processing of gastrointestinal inputs by the vagus nerve. For selective targeting of vagal sensory neurons with terminals in intestinal villi, we sought to exploit the presumed role for vagal GLP1R in nutrient detection. We generated *Glp1r-ires-Cre* mice and adapted genetic approaches to map, image, and control vagal GLP1R neurons. Surprisingly, vagal GLP1R neurons do not densely target intestinal villi but instead display characteristic IGLE terminals and function as gastrointestinal mechanoreceptors. Most sensory neurons that innervate intestinal villi instead contain another receptor, GPR65. Vagal GPR65 neurons are insensitive to GLP1 or cholecystokinin, but instead detect serotonin, and in vivo imaging reveals broad responses to meal-associated stimuli in the intestinal lumen. The central projections of GPR65 neurons are remarkably specific, and optogenetic activation of GPR65 neurons causes a powerful blockade of gastric contractions without impacting breathing or heart rate, which are also under vagal control. Genetic access to different neural populations that monitor and control gastrointestinal physiology has provided direct links between neuronal identities, peripheral terminal morphologies, central projection fields, response properties, hormone sensitivities, and physiological functions.

RESULTS

Imaging Single Neuron Responses in Vagal Ganglia In Vivo

We developed an in vivo calcium imaging approach in vagal ganglia to study the peripheral representation of autonomic inputs. Genetically encoded calcium indicators, such as GCaMP3, have provided an optical proxy for activity-dependent calcium transients in many neuron types, including peripheral sensory neurons (Barretto et al., 2015; Kim et al., 2014). In vivo calcium imaging enables a massively parallel analysis of single neuron responses and is compatible with genetic marking techniques for neuron identification.

In initial experiments, GCaMP3 expression was driven using a Cre driver line (*Vglut2-ires-Cre*) that targets all vagal sensory neurons (Chang et al., 2015) and a Cre-dependent reporter allele (*lox-GCaMP3*); in some experiments, an alternate Cre driver line (*E2a-Cre*) was used that resulted in a constitutive *GCamp3* allele (*Rosa26-GCaMP3*). Vagal ganglia were surgically exposed for in vivo imaging through a ventral incision in the neck with connections to peripheral organs intact (Figures 1A and 1B). Approximately 150 neurons were analyzed in parallel per imaging field by confocal microscopy, with neurons remaining viable and stably imaged for over 6 hr. Neuron viability was determined after each session by electrical stimulation of the nerve trunk, applied as a series of increasing voltage steps (Movie S1). Ganglion imaging was performed during various end-organ stimulations, including (1) gastric distension, (2) duodenal nutrient application, (3) intestinal distension, and (4) lung inflation (Figures 1C–1E).

First, gastric mechanoreceptors were activated by stretching the stomach with a surgically implanted balloon or by infusion of nitrogen gas. Single neurons responded rapidly and reproducibly, and response magnitude correlated with the extent of gastric distension (Figure S1). Volume expansion by 300 μl mimicked meal-induced distension and activated 16.8% (198/1,181, ten mice) of imaging-accessible vagal sensory neurons. Gastric mechanoreceptors accounted for nearly all neurons (92%, 56/62) responsive to liquid diet infusion into the stomach after sealing the pyloric sphincter (Figures 1E and S1), consistent with prior evidence that the stomach lacks chemoreceptors for nutrients (Powley and Phillips, 2004).

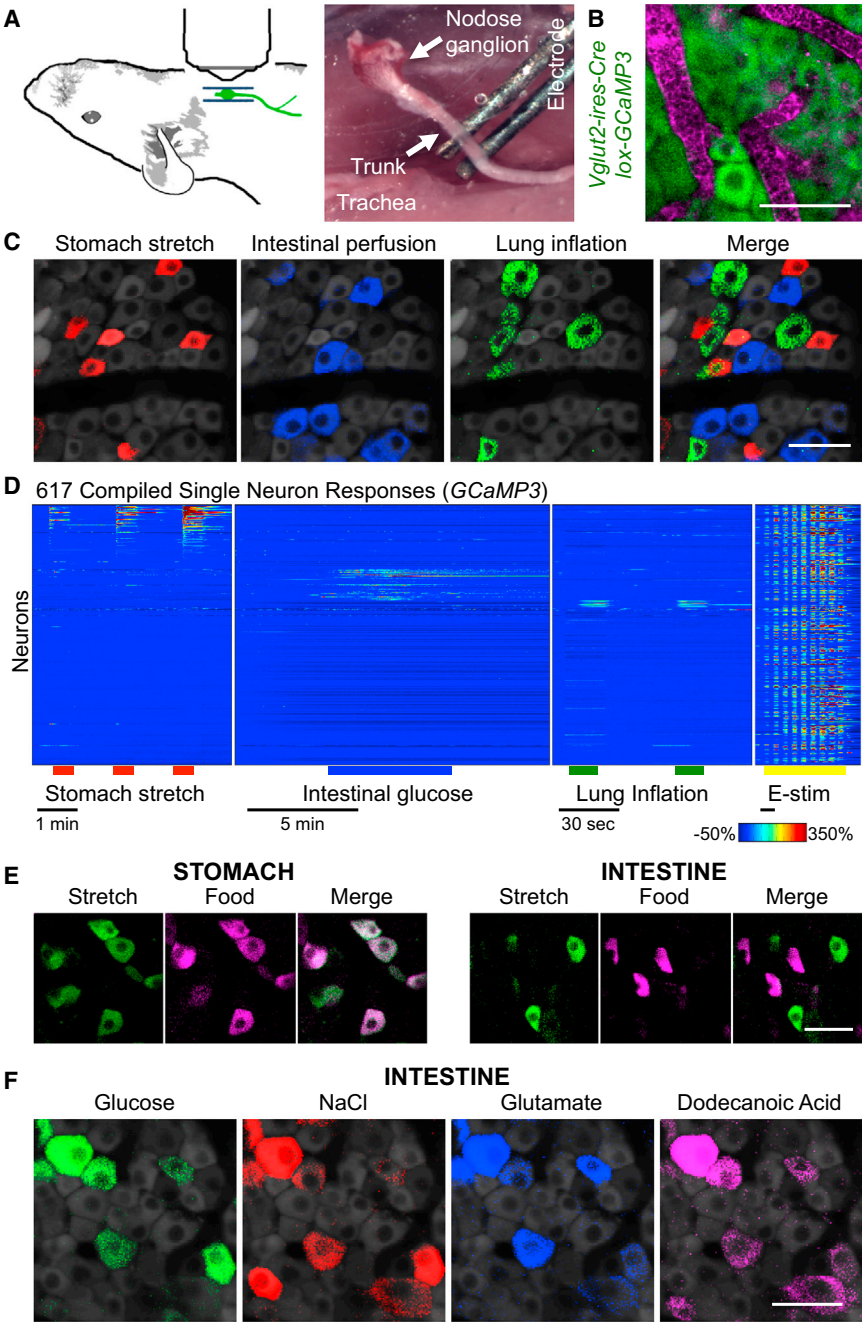

Figure 1. In Vivo Imaging of Vagal Sensory Neurons

(A) Cartoon and photograph of imaging preparation.

(B) Whole mount image of GCaMP3 fluorescence (green) and blood vessels (magenta, intravenous Evans blue) in vagal ganglia.

(C) GCaMP3 fluorescence signal in vagal ganglia during stomach stretch (red), intestinal NaCl perfusion (blue), and lung stretch (green).

(D) Time-resolved responses (ΔF/F, color scale) of 617 neurons (one neuron per row) to stimuli indicated. E-stim time scale bar, 30 sec.

(E and F) GCaMP3 fluorescence signal in vagal ganglia during (E) organ stretch (nitrogen, saline), food injection (liquid diet), or (F) intestinal perfusion of glucose (1 M, saline), sodium chloride (500 mM, saline), sodium glutamate (500 mM, saline), and dodecanoic acid (25 mM, saline and conjugated mouse bile). Scale bars, 50 μm.

See also Figures S1 and S2 and Movie S1.

Second, intestinal chemoreceptors were activated by either perfusing or injecting liquid diet into the proximal small intestine near the gastro-duodenal junction. Perfused stimuli were administered through a surgically implanted cannula in the duodenal bulb with a stimulus exit port located ~11 cm distally. Injection of liquid diet (200 μl) activated 11.1% of imaging-accessible sensory neurons (87/780 neurons, six mice). Isotonic saline (200 μl) did not evoke calcium transients, suggesting that these responses were not due to mechanosensation (Figure S1). Most individual neurons displayed broad responses to many stimuli, including intestinal glucose, glutamate, fatty acids, salt, and low pH, consistent with polymodal signal integration (Figures 1F and S1). Responses were not observed to the artificial sweetener saccharin at concentrations that activate the sweet taste receptor complex (Figure S1).

Third, mechanical stretch of the intestine was evoked by injecting a larger bolus of isotonic saline into the proximal intestine after clamping the exit port to prevent fluid release. This preparation resulted in a controlled distension of the intestine that was visually observed and alleviated by unclamping the exit port. Intestinal distension activated a subset of vagal sensory neurons (26%; 131/503, four mice), and in control experiments, the bolus of isotonic saline did not activate vagal afferents in the absence of an exit port clamp. Intestinal stretch and intestinal nutrients predominantly activated discrete sensory neuron cohorts (Figures 1E and S1).

Fourth, airway mechanoreceptors were activated by introducing nitrogen or ambient air through a tracheal cannula to inflate the lung. Lung inflation evoked rapid, robust, and reproducible calcium transients in 3.6% (28/762, six mice) of imaging-accessible sensory neurons. Lung inflation by ambient air, oxygen, and nitrogen activated the same neurons, suggesting a mechanosensory response indifferent to airway oxygen levels (Figure S2). Responses were typically sustained for the entire stimulus duration and terminated abruptly when airway pressure was reduced. Consistent with prior studies, lung stretch-responsive neurons were cyclically active during tidal breathing, detecting lung expansion with each breath (Figure S2). These findings indicate that in vivo calcium imaging in vagal ganglia can reliably report on physiological stimuli over a timescale as rapid as tidal breathing.

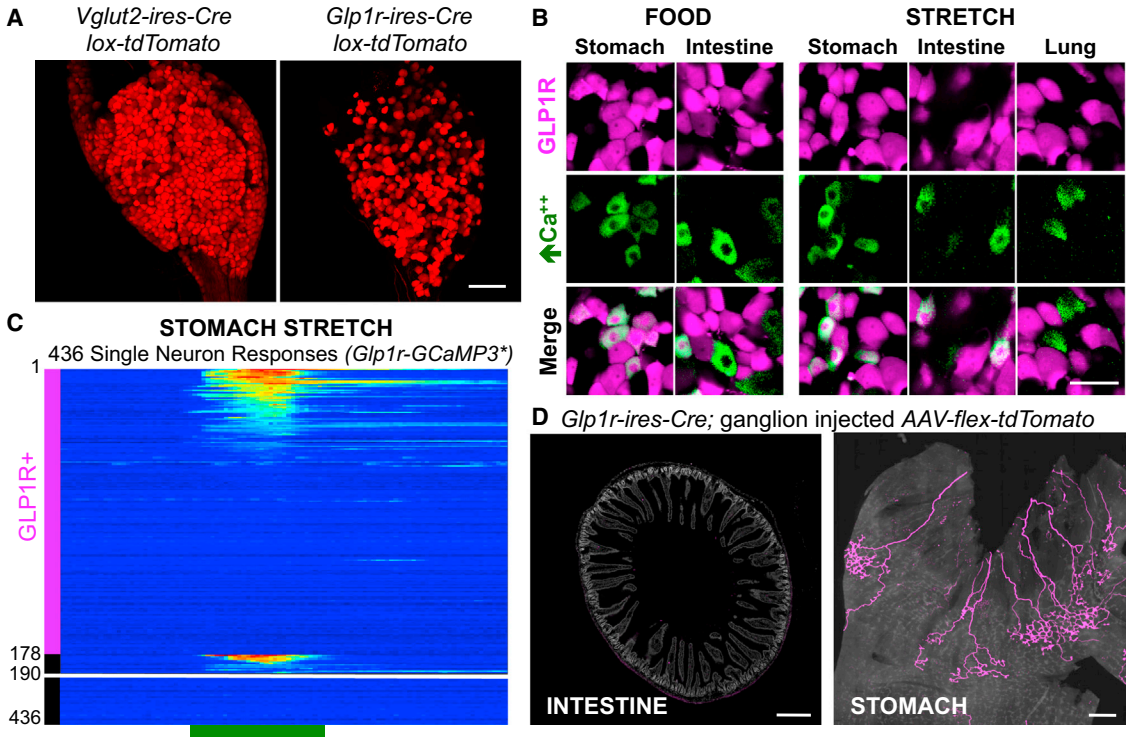

Figure 2. Vagal GLP1R Neurons Are Mechanoreceptors

(A) Whole mount tdTomato fluorescence in vagal ganglia from knockin mice. Scale bar, 100 μm.

(B) Tomato fluorescence indicating GLP1R neurons (magenta) and GCaMP3 fluorescence responses to stimuli indicated (green) in vagal ganglia of *Glp1r-GCaMP3** mice.

(C) Time-resolved responses (ΔF/F, color scale) of 178 GLP1R neurons and 258 other neurons (12 depicted that responded) to gastric distension (green bar, 30 seconds) induced by nitrogen perfusion. Only some unresponsive tdTomato-negative neurons are depicted. Numbers at y axis base indicate total number of viable imaged neurons.

(D) AAV mapping of GLP1R neuron projections in intestine and stomach. Scale bars, 500 μm (left), 1 mm (right).

See also Figures S3 and S4.

Different vagal sensory neurons responded to stomach stretch, intestinal nutrients, and lung inflation, indicating that individual vagal sensory neurons have specific response properties. In vivo imaging also provides positional information about responsive neurons. Sensory neurons were intermingled without any apparent spatial clustering based on response properties (Figure S2), consistent with a salt-and-pepper organization of vagal inputs.

Vagal GLP1R Neurons Are Gastrointestinal Mechanoreceptors

Vagal GLP1R neurons co-express multiple gut hormone receptors (Figure S3) based on two-color fluorescence in situ hybridization (FISH), raising the possibility that these neurons provide an integrated nutrient response. To examine whether these neurons sense gastrointestinal inputs, we tagged them genetically during in vivo imaging experiments. We generated *Glp1r-ires-Cre* knockin mice in which Cre recombinase is expressed from the endogenous *Glp1r* locus using an internal ribosome entry site (IRES) sequence (Figures 2A and S3). Expression of Cre-dependent reporters in *Glp1r-ires-Cre* mice was observed in many cell types that contain GLP1R (Baggio and Drucker, 2007), and two-color analysis validated that appropriate cells were targeted (Figure S3). We noted an increase in fluorescent cells visualized in vagal ganglia of *Glp1r-ires-Cre*; *lox-tdTomato* mice, likely due to inefficient detection of low-level or transient *Glp1r* transcript by FISH.

To measure the response properties of vagal GLP1R neurons, we generated a triple knockin mouse line: *Glp1r-ires-Cre; lox-tdTomato; Rosa26-GCaMP3* (*Glp1r-GCaMP3**) in which all sensory neurons expressed GCaMP3 from a constitutive allele, and GLP1R neurons were visualized by tdTomato expression. Responses of vagal GLP1R neurons to gastric distension, intestinal nutrients, intestinal distension, and lung inflation were queried by in vivo ganglion imaging in *Glp1r-GCaMP3** mice (Figures 2B, 2C, and S4). We observed only rare vagal GLP1R neurons that responded to lung inflation (1%, 2/204, four mice) and some that detected liquid diet (200 μl) injected in the duodenal bulb (9.2%, 18/195, three mice). Instead, unexpectedly, GLP1R neurons accounted for most neurons responsive to gastric distension (81%, 46/57, three mice). Furthermore, a separate cohort of GLP1R neurons accounted for most neurons responsive to saline-induced intestinal distension (67.7%, 88/130, two mice). Stomach and intestinal stretch activated discrete subsets of

vagal GLP1R neurons, with other vagal GLP1R neurons likely detecting different physiological stimuli. GLP1R neurons thus account for most vagal mechanoreceptors in stomach and intestine, while nutrient responses occur predominantly in GLP1R-negative neurons.

GLP1R Neurons Form IGLEs in Stomach Muscle

Next, we asked where vagal GLP1R neurons project in the gastrointestinal tract. We previously developed a genetic approach involving adeno-associated viruses (AAVs) to map vagal sensory neuron anatomy (Chang et al., 2015). Cre-dependent AAVs encoding a fluorescent reporter (*AAV-flex-tdTomato*) were injected into vagal ganglia of knockin mice, and labeled fibers were visualized in peripheral tissues by whole mount fluorescence and/or immunohistochemistry. AAV infections occurred in ~50% of vagal sensory neurons, without apparent preference for particular neuron classes or targeting of passing motor fibers (Chang et al., 2015).

We infected vagal ganglia of *Glp1r-ires-Cre* mice with *AAV-flex-tdTomato* and visualized tdTomato-containing fibers in the periphery (Figures 2D and S4). In the intestine, vagal GLP1R neurons were largely confined to intestinal muscle (Figure S4) and surprisingly did not densely innervate villi in the proximal duodenum. Quantitative analysis involving normalization with a Cre-independent GFP reporter virus (*AAV-GFP*) revealed that the vast majority of vagal afferents innervating intestinal villi (94.2% ± 2.2%, n = 6) did not contain GLP1R. Vagal GLP1R neurons instead densely innervated stomach muscle. The extent of innervation was quantified by counting the number of enteric ganglia contacted by labeled IGLEs in *Vglut2-ires-Cre* and *Glp1r-ires-Cre* mice. AAV infections occurred unilaterally in the left ganglion, which innervates the ventral half of the stomach. We counted 101 ± 17 enteric ganglia innervated by labeled IGLEs per ventral stomach in *Vglut2-ires-Cre* mice and 131 ± 38 in *Glp1r-ires-Cre* mice, suggesting that vagal GLP1R neurons account for most vagal IGLEs in stomach muscle.

Optogenetic Control of Gut Motility

Vagal GLP1R neurons do not densely innervate intestinal villi, so we sought to identify other neuron types that do and might be relevant for gastrointestinal function. We previously used a genome-based strategy to identify G protein-coupled receptors (GPCRs) expressed in vagal sensory neurons (Chang et al., 2015) and found two other GPCRs that mark small neuronal subsets: the purinergic receptor P2RY1 and the orphan receptor GPR65. P2RY1 neurons target the lung, forming stereotyped candelabra terminals at neuroepithelial bodies, and optogenetic activation of vagal P2RY1 neurons acutely silences breathing (Chang et al., 2015). In contrast, vagal neurons containing GPR65 do not densely innervate the lung (Chang et al., 2015), and their physiological function remained unknown.

We used optogenetics to ask whether any of these neurons might control gastrointestinal physiology (Figure 3). We crossed *Glp1r-ires-Cre*, *Gpr65-ires-Cre*, *P2ry1-ires-Cre*, and *Vglut2-ires-Cre* mice with a Cre-dependent channelrhodopsin allele (*lox-ChR2;* offspring of *Marker-Cre* mice are called *Marker-ChR2*). Neuron activity was evoked in anesthetized mice by focal illumination of the vagus nerve trunk, and robust light-induced action potentials were observed in *Vglut2-ChR2*, *P2ry1-ChR2*, *Glp1r-ChR2*, and *Gpr65-ChR2* mice. Most vagal GLP1R and GPR65 neurons (>95%, >97%) are slow-conducting C fibers, as revealed by measuring neuron conduction velocities at fixed intervals from the illumination site (Figure S5).

Activating all vagal sensory neurons in *Vglut2-ChR2* mice caused profound and immediate drops in breathing rate, heart rate, and gastric pressure (Chang et al., 2015). In contrast, activating vagal GPR65 neurons caused a striking light-induced blockade of gastric contractions, without impacting breathing or heart rate. Gastric contractions occurred at a frequency of 3.4 ± 0.3 per minute in control *lox-ChR2* mice, and this frequency was not altered by vagus nerve illumination (3.4 ± 0.6 per minute, six mice). In *Gpr65-ChR2* mice, gastric contractions occurred at a similar frequency at rest (3.1 ± 0.3 per minute, five mice), but optogenetic activation stopped or reduced gastric contractions during a 1-min (0 ± 0.0 per minute, five mice) and 3-min (0.6 ± 0.3 per minute, three mice) photostimulation period. Activating GPR65 neurons decreased both tonic and phasic measurements of gastric pressure. GPR65 is not expressed in vagal motor neurons, indicating that these effects are due to sensory neuron stimulation. Activating vagal GLP1R neurons instead caused a different response characterized by increased gastric pressure and also produced a small but significant change in breathing and heart rate, suggesting that some vagal GLP1R neurons communicate with organ systems other than the gut. The strikingly selective response to GPR65 sensory neuron activation strengthens the conclusion that the vagus nerve consists of several co-fasciculating classes of sensory neurons (so-called "labeled lines"), each of which conveys a highly specific signal relevant for autonomic physiology.

GPR65 Neurons Target Intestinal Villi

Optogenetic studies suggested that GPR65 neurons receive inputs from the gastrointestinal tract. GPR65, P2RY1, and GLP1R mark subsets of neurons, with FISH revealing expression in 10.2%, 11.6%, and 11.5% of sensory neurons (Chang et al., 2015); the *Glp1r* probe provided lower signal-to-noise and may not reveal all neurons containing *Glp1r* mRNA. Two-color FISH indicated that GPR65 neurons are distinct from GLP1R and P2RY1 neurons (Figure 4A). Nearly all GPR65 neurons lacked GLP1R (99.5%, 220/221) and nearly all GLP1R neurons lacked GPR65 (99.5%, 198/199); similarly orthogonal results were obtained in pairwise analyses involving P2RY1 (Figure S5).

The peripheral projections of vagal GPR65 neurons were mapped by infecting vagal ganglia of *Gpr65-ires-Cre* mice with *AAV-flex-tdTomato*. GPR65 neurons display extensive innervation of intestinal villi in the duodenal bulb immediately adjacent to the pyloric sphincter (Figure 4B). Innervation density of GPR65 neurons decreases dramatically beyond the duodenal bulb, with only sparse innervation of the rest of the duodenum and small intestine. Consistent with these findings, bulk labeling of vagal sensory neurons reveals maximal innervation of villi within the first 1–3 cm of duodenum (Figure 4C). Quantitative analysis (Figure 4E) revealed that GPR65 neurons accounted for most vagal innervation of duodenal villi (57.4% ± 11.9%, n = 6) while as described before, GLP1R neurons did not. Orthogonal results were obtained in stomach muscle, where GPR65 neurons only accounted for 6 ± 4 enteric ganglia innervated by labeled

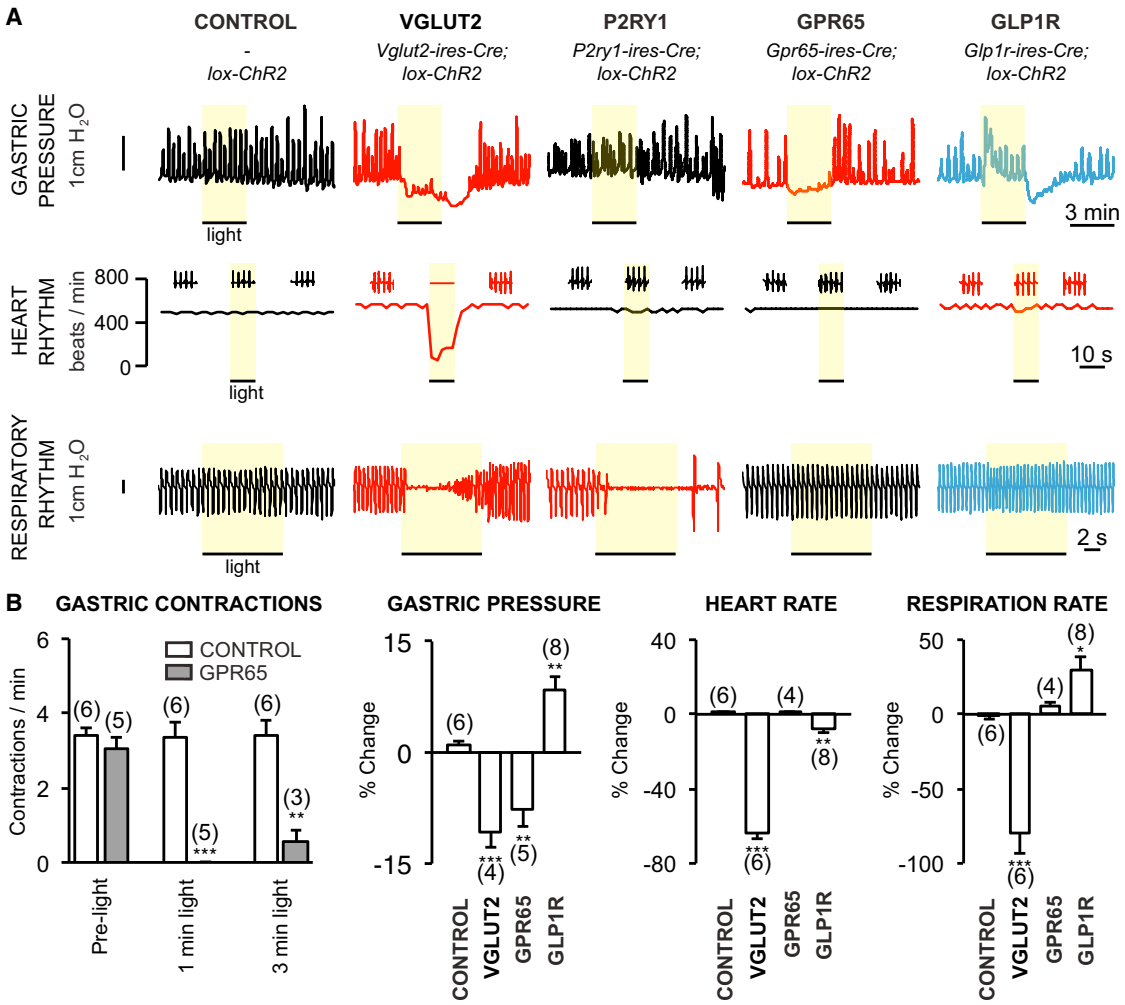

Figure 3. Optogenetic Control of Gut Motility

(A) Physiological responses to optogenetic activation (yellow bar) of vagal sensory neuron subtypes.

(B) Quantification of physiological changes to neuron subtype stimulation (mean ± SEM, n = 3–8, *p < 0.05, **p < 0.01, ***p < 0.001).

See also Figure S5.

IGLEs per ventral stomach. Thus, GLP1R and GPR65 neurons display strikingly distinct anatomical projections within the gastrointestinal tract, with GPR65 terminals enriched in villi of intestinal mucosa and GLP1R neurons largely confined to stomach and intestinal muscle.

GPR65 Neurons Detect Serotonin In Vitro and Intestinal Nutrients In Vivo

Genetically defining vagal sensory neurons in intestinal villi allows for a controlled analysis of neuron response properties. We next asked whether GPR65 neurons detect various gut hormones (Figure 5). Responses were imaged using the calcium indicator Fura-2 in acute vagal ganglia cultures from heterozygous knockin/knockout mice containing a *GFP* allele at the endogenous *Gpr65* locus (*Gpr65*$^{GFP/+}$) (Radu et al., 2006). For comparison, GLP1R neurons were analyzed using *Glp1r-ires-Cre*; *lox-L10-GFP* mice (Figure S6). Serotonin (or a specific agonist for the serotonin receptor HTR3A) activated most GPR65 neurons (58%, 15/26), while cholecystokinin did not (2%, 1/41). Two-color FISH revealed that GPR65 neurons predominantly represent a subset of HTR3A-containing neurons and most do not express the cholecystokinin receptor CCKAR (Figure 5D). In contrast, cholecystokinin activated many vagal GLP1R neurons (62%, 53/85), consistent with co-expression of these gut hormone receptors (Figures S3 and S6), while serotonin activated some (19%, 16/85). Likewise, the TRPV1 agonist capsaicin activated most GLP1R neurons (68%, 58/85) but only rare GPR65 neurons (9%, 3/34). We did not observe acute responses to GLP1R agonists in any vagal sensory neurons by in vitro calcium imaging, or by in vivo ganglion imaging following intraperitoneal (IP) injection (Figure S6), suggesting a modulatory or developmental role for GLP1R in vagal afferents. Prior studies reporting vagal responses to GLP1R agonists required intravenous agonist

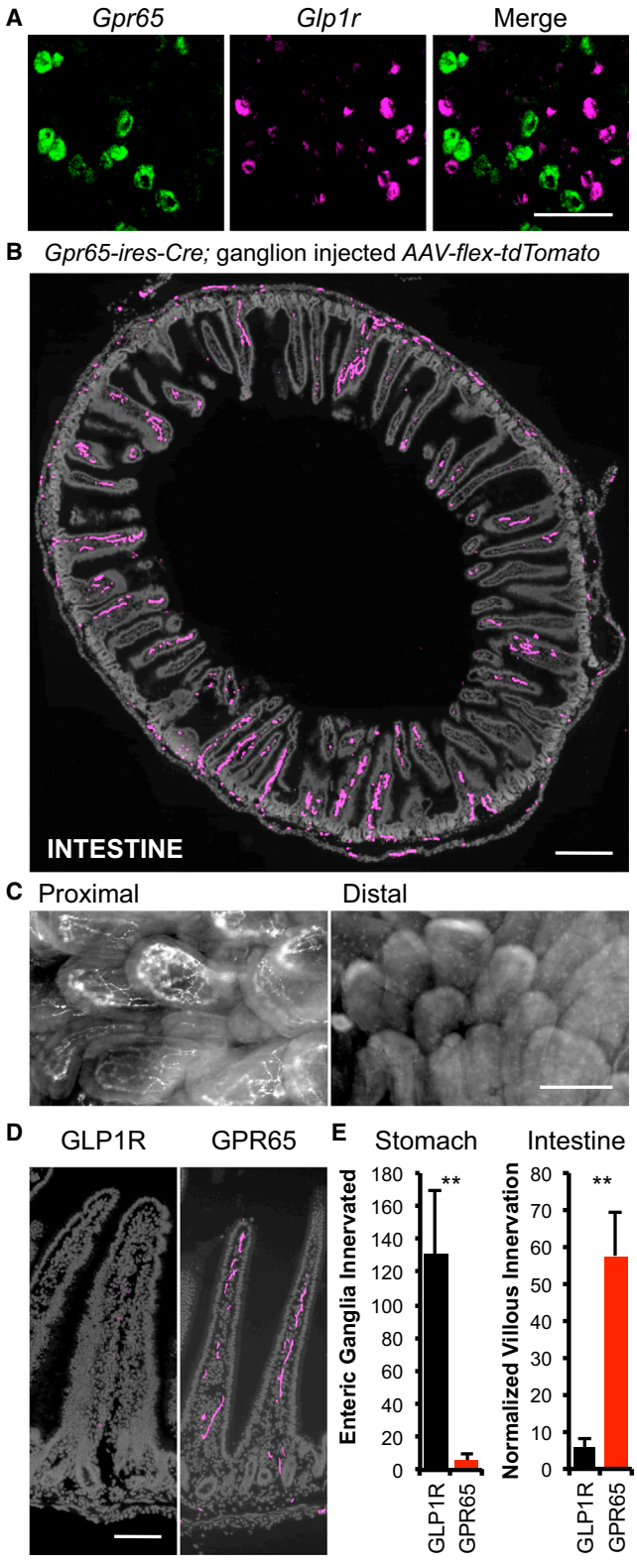

Figure 4. GPR65 Neurons Target Intestinal Villi

(A) Two-color FISH in vagal ganglia reveals expression of *Gpr65* and *Glp1r* in different sensory neurons. Scale bar, 100 μm.

(B) Vagal sensory neuron projections were mapped by infecting vagal ganglia of *Gpr65-ires-Cre* mice with *AAV-flex-tdTomato*. Terminals were visualized by immunofluorescence of duodenum (cryosections) and intestinal architecture visualized with DAPI (gray). Scale bar, 500 μm.

(C) Whole mount fluorescence of nerve terminals in an en face preparation of proximal (<1 cm from pylorus) and distal (4 cm from pylorus) intestinal villi after injecting vagal ganglia of *Vglut2-ires-Cre* mice with *AAV-flex-tdTomato*. Scale bar, 100 μm.

(D) High-magnification image of villi innervation. Scale bar, 100 μm.

(E) Numbers of intestinal villi and gastric enteric ganglia innervated by vagal sensory neuron types were counted, and for villi, normalized using a Cre-independent reporter (mean ± SEM, n = 6, **p < 0.01).

See also Figure S5.

administration, and responses were delayed for minutes, consistent with indirect rather than direct activation of afferents or efferents (Bucinskaite et al., 2009). Taken together, these findings indicate a prominent role for serotonin sensation but not CCK or GLP1 sensation by GPR65-expressing vagal afferents, which represent the major species in intestinal villi. GPR65 afferents likely communicate with enterochromaffin cells, the principal source of serotonin in the body.

Responses of GPR65 neurons to physiological stimuli were measured by in vivo calcium imaging in vagal ganglia of *Gpr65-GCaMP3** mice (Figure 6). GPR65 neurons did not account for most neurons detecting lung inflation (0/48, 3 mice), saline-induced intestinal distension (6.3%, 3/47, 3 mice), or balloon-induced stomach stretch (5.6%, 4/72, 3 mice). Instead, GPR65 neurons accounted for most neurons responsive to liquid diet (200 μl) injected into the duodenal bulb (66%, 27/41, 4 mice). Only rare responses were observed to nutrients perfused through distal regions of the duodenum that did not include the duodenal bulb (Figure S6). Taken together with anatomical data, GPR65 neurons with terminals embedded in villi adjacent to the pyloric sphincter account for most vagal chemoreceptors responsive to intestinal nutrients.

Central Representations of Vagal Inputs from the Gastrointestinal Tract

Next, we used AAV mapping to ask whether GPR65 and GLP1R inputs are segregated centrally (Figure 7). We simultaneously infected vagal ganglia of *Gpr65-ires-Cre* and *Glp1r-ires-Cre* mice with *AAV-flex-tdTomato* and *AAV-GFP*. GFP signal revealed axons of all vagal sensory neuron types in the nucleus of the solitary tract (NTS) and area postrema, while tdTomato signal specifically labeled GPR65 and GLP1R axons. GLP1R and GPR65 axons segregate to topographically distinct regions of the posterior NTS (Figure 7; Figure S7 for entire rostral-caudal series). Vagal GLP1R neurons predominantly target the medial NTS subnucleus, a region that receives input from gastric mechanoreceptors (Willing and Berthoud, 1997). In contrast, GPR65 neurons projected more medially to the NTS commissural zone, just beneath the area postrema. For a direct comparison of GLP1R neuron (tdTomato) and GPR65 neuron (GFP) projection patterns (Figure 7C), vagal ganglia of *Glp1r-ires-Cre*; *Gpr65*$^{GFP/+}$ mice were infected with *AAV-flex-tdTomato*. This strategy revealed that vagal GLP1R and GPR65 neurons target adjacent but distinct NTS subregions, suggesting engagement of different neural circuits.

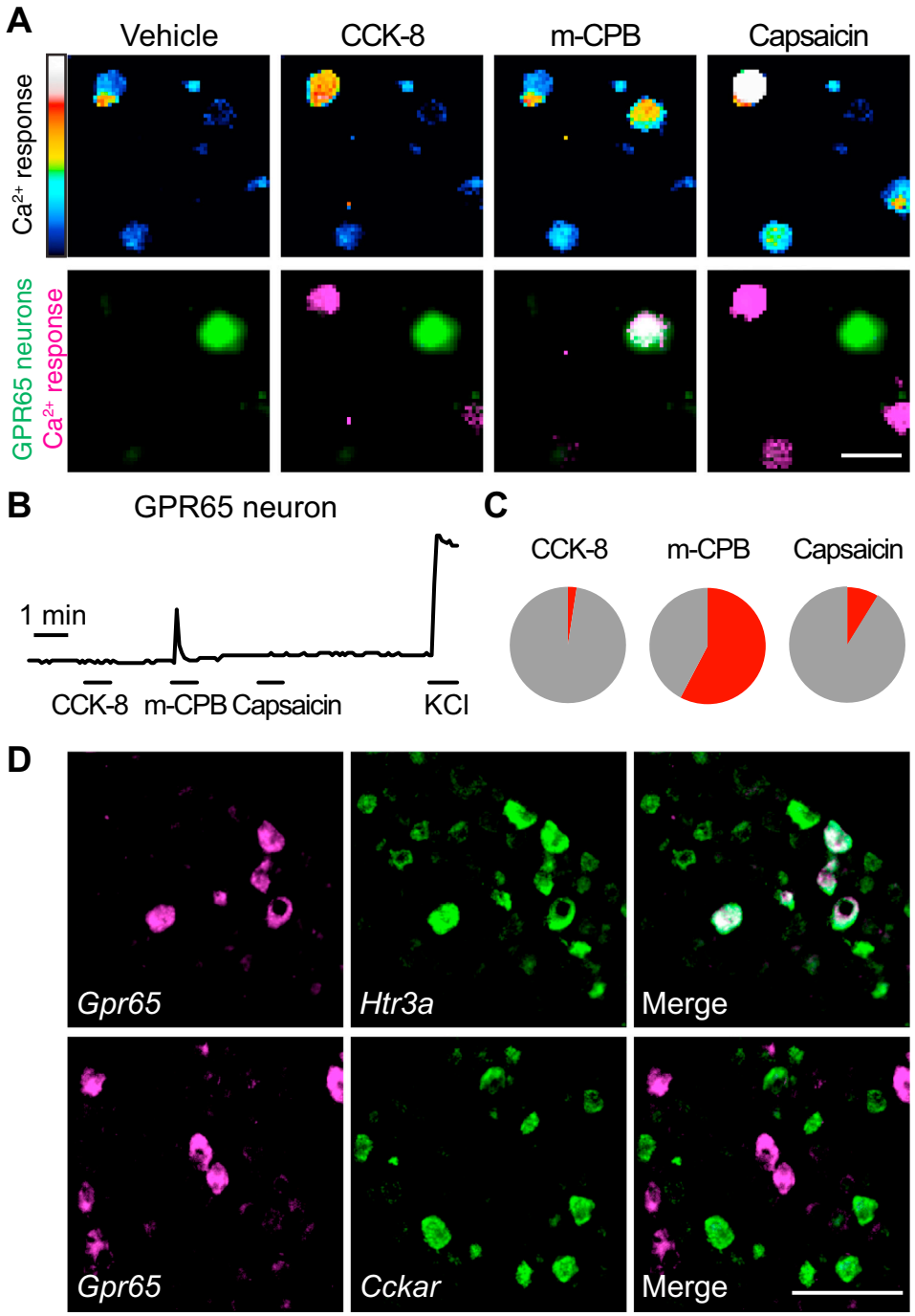

Figure 5. GPR65 Neurons Respond In Vitro to an HTR3A Agonist

(A) Calcium responses by Fura-2 imaging of dissociated vagal sensory neurons from *Gpr65*$^{GFP/+}$ mice to CCK-8 (10 nM), the HTR3A agonist *m*-chlorophenylbiguanide (mCPB, 100 μM) and capsaicin (1 μM). Scale bar, 40 μm. Top: Fura-2 excitation. Bottom: GFP fluorescence (green) and calcium responses (magenta).

(B) Representative responses of a GPR65 neuron.

(C) Pie chart indicating percentage of GPR65 neurons activated (red) by each ligand.

(D) Two color FISH in vagal ganglia. Scale bar, 100 μm.

See also Figure S6.

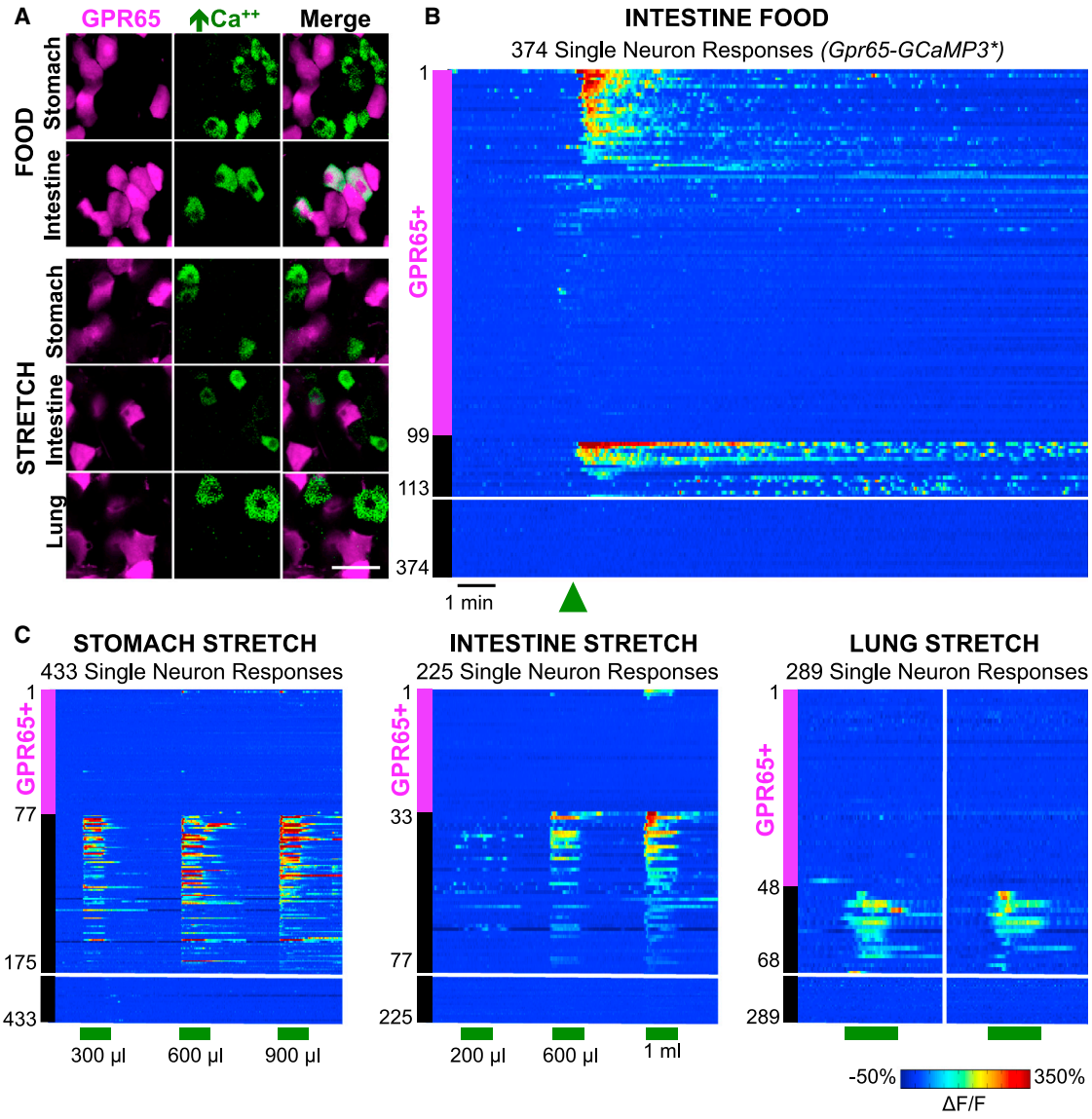

Figure 6. GPR65 Neurons Detect Intestinal Nutrients In Vivo

(A) In vivo imaging of vagal ganglia in *Gpr65-GCaMP3** mice showing GCaMP3 responses (green) of GPR65 neurons (magenta) to stimuli indicated. Scale bar, 50 µm. (B and C) Rows indicate time-resolved responses (ΔF/F, color coded) of single neurons in *Gpr65-GCaMP3** mice to stimuli (green arrow: food injection; green bars: 30 s stomach and intestine, 15 s lung). Magenta and black bars represent tdTomato-positive and negative neurons. Only some unresponsive tdTomato-negative neurons are depicted; numbers at y axis base indicate total number of viable imaged neurons.

See also Figure S6.

DISCUSSION

Internal sensory neurons of the vagus nerve survey the state of several major physiological systems. Within the gastrointestinal tract, sensation of gastric distension and intestinal nutrients are long-appreciated signals that activate vagal afferents and impact physiology and behavior. Here, we genetically define sensory neurons that detect these cues and use Cre-based anatomical mapping, in vivo imaging, and optogenetics to decipher aspects of gut-to-brain signaling.

One small group of vagal afferents marked by expression of the receptor GPR65 (~230 neurons per ganglion) innervates villi in the proximal small intestine close to the gastro-duodenal junction. GPR65 neurons respond to serotonin, but not other gut hormones such as GLP1 and cholecystokinin. In vivo calcium imaging revealed acute responses of GPR65 neurons to food introduced into the intestinal lumen, providing a direct functional link between sensory neurons with terminal fields in intestinal villi and nutrient detection. Responses of vagal GPR65 neurons to nutrients were rapid and transient, presumably turning off as peristaltic movements removed stimuli from the duodenal bulb.

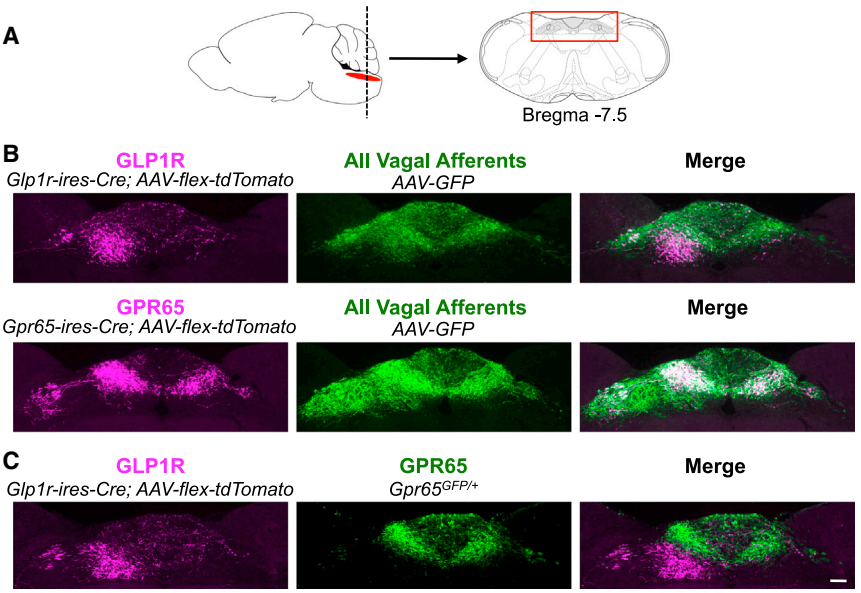

Figure 7. Visualizing Brainstem Innervation

(A) Vagal sensory neuron axons were analyzed in a brainstem region (red box) containing the NTS and area postrema.

(B) Vagal ganglia of *Glp1r-ires-Cre* and *Gpr65-ires-Cre* mice were infected with *AAV-flex-tdTomato* and *AAV-GFP* for immunofluorescence-based detection of Cre-containing (magenta) and all (green) vagal sensory neuron axon types.

(C) Vagal ganglia of *Glp1r-ires-Cre; Gpr65*$^{GFP/+}$ mice were infected with *AAV-flex-tdTomato* for simultaneous visualization of GLP1R (magenta) and GPR65 (green) axons. Scale bar, 100 μm.

See also Figure S7.

Artificial sweeteners perfused through the duodenum did not evoke a response in vagal sensory neurons, suggesting that any metabolic responses mediated by intestinal sweet receptors involve alternative pathways (Jang et al., 2007). Vagal GPR65 neurons accounted for most but not all nutrient-responsive neurons, indicating at least one other class of nutrient-responsive vagal afferent.

The ability of vagal GPR65 neurons to slow gastric motility suggests a two-pronged response to nutrient-evoked serotonin release in the duodenal bulb. During a meal, food is released through the pyloric sphincter into the duodenal bulb. When a critical level is reached in the duodenal bulb, as detected by a deflection in osmolarity, pH, and/or mechanical brushing, a burst of serotonin is released. Serotonin is a classic signal that promotes gut motility through the enteric nervous system, propelling resident contents distally to sites of enzyme secretion and absorption (Bertrand and Bertrand, 2010). Simultaneously, serotonin-responsive GPR65 neurons of the vagus nerve initiate an intestine-brain-stomach circuit that causes a striking feedback blockade of gastric motility, decreasing entry of new content into the duodenal bulb. This dual activity of serotonin should purge the proximal intestine of contents. After the first bolus has migrated, the system presumably re-sets and re-fills to prepare the next bolus. Based on these findings, we propose an important role for vagal GPR65 neurons in controlling the pulsatile rhythm of food entry into the intestine. Optogenetics enables a specific analysis of vagal chemosensors in the intestine that was not possible with sham feeding, which triggers a complex response involving multiple vagal afferent types but also enteric neurons, spinal neurons, circulating hormones, and direct nutrient effects. Whole nerve stimulations also do not distinguish contributions from villous neurons, gastrointestinal mechanoreceptors, motor neurons, or other fiber types. Future studies are needed to determine the role of GPR65 itself in intestinal homeostasis, as these studies reveal it to be a prime candidate for regulating gastrointestinal physiology. Specific targeting of GPR65 neurons may impact disorders of nutrient absorption and gut motility, such as dyspepsia and ileus.

Genetically guided anatomical tracing showed the central representation of nutrient-responsive vagal afferents containing GPR65. Anterograde tracing studies from the intestine using bulk tracing techniques are technically challenging and have not enabled differential analysis of fiber type-specific projection fields, such as those from chemoreceptors and mechanoreceptors. Immediate early gene (IEG) analysis in the NTS suggested a relatively broad topographical domain responsive to intestinal nutrients (Phifer and Berthoud, 1998). However, nutrient-evoked IEG induction potentially includes direct or indirect contributions from multiple vagal afferent types, as well as enteric neurons, spinal neurons, hormones, and circulating nutrients themselves. Experiments here instead reveal strikingly restricted central projections of vagal GPR65 neurons that are confined to the commissural NTS. This projection field is distinct from that of gastrointestinal mechanoreceptors (Figure 7) and apnea-promoting pulmonary afferents (Chang et al., 2015), consistent with a topographical NTS map linked to physiological input. Revealing the spatially confined projections of vagal GPR65 neurons highlights the power of using genetic tools for selective visualization of afferent subtype-specific terminal fields in the brainstem.

Four findings suggest that villous nutrient detection by the vagus nerve occurs primarily through GLP1R-independent mechanisms. Vagal GLP1R sensory neurons (1) do not account for most nutrient-responsive neurons, (2) do not densely innervate intestinal villi, (3) do not respond to GLP1R agonists in vitro, and (4) do not respond to GLP1R agonists administered intraperitoneally by in vivo ganglion imaging. Instead, a cohort of vagal GLP1R neurons forms IGLE terminals in stomach and accounts for most gastric stretch receptors by in vivo imaging. Furthermore, vagal GLP1R neurons project centrally to medial NTS regions that show IEG induction following gastric distension (Willing and Berthoud, 1997). The same genetically defined neuron type forms IGLEs and senses stomach stretch, supporting the model that IGLEs are mechanosensitive terminals (Zagorodnyuk et al., 2001). A second cohort of vagal GLP1R neurons responds to intestinal distention, indicating that vagal GLP1R

neurons generally account for several classes of gastrointestinal mechanoreceptors.

Intriguingly, these studies add to the list of gut hormone receptors expressed by gastric mechanoreceptors. In some studies, but not all, cholecystokinin was reported to activate the same sensory neurons that detect gastric distension (Blackshaw and Grundy, 1990; Schwartz et al., 1991). One caveat is that cholecystokinin exerts profound effects on gastric motility and tone, effects that might secondarily impact stretch sensitivity. Here, analyzing responses of genetically defined gastrointestinal mechanoreceptors in cell culture reveals acute and direct cholecystokinin-evoked calcium transients that are independent of secondary physiological effects. Prior studies also reported that leptin activates gastric mechanoreceptors (Li et al., 2011) while ghrelin inhibits them (Page et al., 2007). One model is that gut hormones relay convergent state-dependent information about ingested and stored nutrients to modulate the sensitivity of gastric stretch sensors. When nutrients are abundant, subthreshold sensitization of gastric mechanoreceptors would promote satiety at lower distension levels; in contrast, when nutrients are scarce, a larger sized meal would be required for the same sensory neuron response. Here, we reveal that GLP1R is also expressed by mechanoreceptors in stomach, as well as intestine. Unlike CCKAR agonists, GLP1R agonists do not acutely activate vagal afferents, suggesting a modulatory role. Intriguingly, introduction of GLP1R agonists directly into the brainstem can gate NTS responses to stomach distension, and a model was proposed involving GLP1R expression in intrinsic NTS neurons (Hayes et al., 2009). Our studies raise the possibility that GLP1R agonists instead, or in addition, directly modulate vagal sensory neuron axons in the brainstem to control presynaptic neurotransmitter release. Together, these findings suggest that gut hormones exert multi-tiered control over gastric stretch sensitivity at different processing levels in the same neuron.

Sensory systems use different strategies to encode peripheral information. For example, the olfactory system can generate a myriad of odor perceptions. To achieve this, odors are encoded by combinations of receptors and sensory neuron types in the periphery. Olfactory sensory neuron inputs are subsequently mixed without apparent topography in olfactory cortex (Wilson and Sullivan, 2011). This organization allows individual cortical neurons to integrate responses from multiple receptors, which is relevant for generating diverse perceptions. In contrast, the gustatory system is more streamlined, with different sensory cells and peripheral neural circuits devoted to perception of sweet, salty, sour, umami, and bitter taste modalities (Barretto et al., 2015). These separate and parallel processing streams for taste inputs in ascending gustatory circuits are termed ''labeled lines.'' Our data indicate that the vagus nerve uses a coding logic that shares many similarities with gustatory nerves. Individual vagal sensory neurons transmit highly specific information from peripheral organs—such as stomach stretch during feeding and lung inflation during breathing. Furthermore, optogenetic stimulation of vagal GPR65 neurons inhibits gastric contractions without impacting breathing or heart rate, suggesting that individual sensory neurons not only monitor but also control particular organ systems. The sensory arm of the vagus nerve thus consists of several co-fasciculating labeled lines dedicated for particular sensory modalities. Moreover, the cell bodies of neurons responsive to different pulmonary and gastrointestinal inputs are intermingled within vagal ganglia in a salt-and-pepper manner, suggesting that spatial information from the periphery is largely not apparent at the level of the ganglion.

Genetically identifying neuron subtypes relevant for physiology and behavior is a major goal of the neuroscience field. Recent advances revealed neuron types involved in numerous perceptions and behaviors, such as touch, itch, hunger, and aggression (Aponte et al., 2011; Bai et al., 2015; Han et al., 2013; Lee et al., 2014). Genetic approaches help paint a comprehensive picture of neuron function that includes gene expression, peripheral anatomy, central anatomy, in vivo and in vitro responsiveness, and physiological function. Here, we genetically define two discrete classes of gut-to-brain afferents that differentially monitor and control the digestive system, providing a pivotal molecular foundation for exploring the sensory biology and neural circuitry associated with gut-to-brain signaling.

EXPERIMENTAL PROCEDURES

All animal procedures complied with institutional animal care and use committee guidelines. *Glp1r-ires-Cre* mice were prepared by BAC recombineering. *Rosa26-GCaMP3* mice were generated by breeding *lox-GCaMP3* with *E2a-Cre* mice (Jackson, 003314) to achieve germline excision and then breeding out the *E2a-Cre* allele. Genotyping, FISH, in vitro calcium imaging, electrophysiology, optogenetics, and physiological measurements were as described previously (Chang et al., 2015), with reagents, minor modifications, and other mouse lines described in the Supplemental Experimental Procedures.

For anatomical mapping, *AAV-flex-tdTomato* and *AAV-GFP* were injected into vagal ganglia of *Gpr65-ires-Cre* and *Glp1r-ires-Cre* mice (Chang et al., 2015). IGLE density was determined in stomach muscle whole mounts with enteric ganglia labeled by Fluorogold (30 mg/kg IP). Normalized villus innervation is the ratio of tdTomato fibers to GFP fibers in duodenal cryosections (12 μm, sampled every mm over the first cm).

For in vivo imaging, vagal ganglia were surgically exposed and immobilized on a stable platform. GCaMP3 fluorescence was measured by confocal microscopy (Leica TCS SP5 II) in single neurons. Electrical stimulation involved steps (10 s, 2-ms pulses at 5 Hz) of increasing voltage (1–70 V). Airway gases were introduced (1 l/min) by a tracheal cannula. Gastric distension was by nitrogen gas (3–6 ml/min, 15 s) or volume-controlled inflation of a surgically implanted balloon. Liquid diet (200 μl, TestDiet LD101) was injected (Figures 1E, 2, 6, S1B, S4, and S6) after pyloric sphincter sealing. Other stimuli (Figures 1C, 1D, 1F, and S1C–S1F) were introduced (4–5 min) during continuous perfusion (saline or stimulus, 125 μl/min) of the intestine (first ~11 cm). Cells were coded as responsive based on stimulus-evoked changes in GCaMP3 fluorescence. See the Supplemental Experimental Procedures for more information about surgery, microscopy, introduction of test stimuli, and data analysis related to in vivo imaging.

For data analysis, sample sizes are indicated in main text, figure legends, or bar graphs (numbers in parentheses). Significance was determined by comparisons to the indicated control group using a two-tailed Student's t test (Figures 2 and 3) or between indicated groups using a two-tailed Mann-Whitney test (Figure 4).

SUPPLEMENTAL INFORMATION

Supplemental Information includes Supplemental Experimental Procedures, seven figures, and one movie and can be found with this article online at http://dx.doi.org/10.1016/j.cell.2016.05.011.

AUTHOR CONTRIBUTIONS

S.D.L., D.E.S., R.B.C., B.D.U., and E.K.W. designed and conceived the study. R.B.C. and E.K.W. made knockin mice. D.E.S., R.B.C., and E.K.W. did the FISH. D.E.S. and B.D.U. did the anatomical studies. R.B.C. did the optogenetics. R.B.C. and E.K.W. did the in vitro imaging. E.K.W. did the in vivo imaging. B.B.L. provided the *Vglut2-ires-Cre* mice. S.D.L., D.E.S., R.B.C., B.D.U., and E.K.W. wrote the manuscript.

ACKNOWLEDGMENTS

We thank David Ginty, Ardem Patapoutian, and John Flanagan for manuscript comments, the Nikon Imaging Center at Harvard Medical Center for microscopy assistance, and the Boston Area Diabetes Research Center Transgenic Core (P30 DK046200) and Boston Area Nutrition Research Center Transgenic Core (P30 DK057521) for generating knockin mice. Funding was provided by the National Institute of Diabetes and Digestive and Kidney Diseases (NIDDK) (RO1 DK103703 to S.D.L.), a National Science Foundation (NSF) pre-doctoral fellowship (to D.E.S.), an F30 NIH training grant (F30CA177170 to E.K.W.), a T32 training grant for the Harvard MSTP program (T32GM007753 to E.K.W.), and the Harvard-MIT Joint Research Grants Program in Basic Neuroscience (to S.D.L. and B.B.L.).

Received: March 12, 2016
Revised: April 11, 2016
Accepted: April 22, 2016
Published: May 26, 2016

REFERENCES

Abbott, C.R., Monteiro, M., Small, C.J., Sajedi, A., Smith, K.L., Parkinson, J.R., Ghatei, M.A., and Bloom, S.R. (2005). The inhibitory effects of peripheral administration of peptide YY(3-36) and glucagon-like peptide-1 on food intake are attenuated by ablation of the vagal-brainstem-hypothalamic pathway. Brain Res. *1044*, 127–131.

Aponte, Y., Atasoy, D., and Sternson, S.M. (2011). AGRP neurons are sufficient to orchestrate feeding behavior rapidly and without training. Nat. Neurosci. *14*, 351–355.

Baggio, L.L., and Drucker, D.J. (2007). Biology of incretins: GLP-1 and GIP. Gastroenterology *132*, 2131–2157.

Bai, L., Lehnert, B.P., Liu, J., Neubarth, N.L., Dickendesher, T.L., Nwe, P.H., Cassidy, C., Woodbury, C.J., and Ginty, D.D. (2015). Genetic identification of an expansive mechanoreceptor sensitive to skin stroking. Cell *163*, 1783–1795.

Barretto, R.P., Gillis-Smith, S., Chandrashekar, J., Yarmolinsky, D.A., Schnitzer, M.J., Ryba, N.J., and Zuker, C.S. (2015). The neural representation of taste quality at the periphery. Nature *517*, 373–376.

Berthoud, H.R., Blackshaw, L.A., Brookes, S.J., and Grundy, D. (2004). Neuroanatomy of extrinsic afferents supplying the gastrointestinal tract. Neurogastroenterol. Motil. *16* (*Suppl 1*), 28–33.

Bertrand, P.P., and Bertrand, R.L. (2010). Serotonin release and uptake in the gastrointestinal tract. Auton. Neurosci. *153*, 47–57.

Blackshaw, L.A., and Grundy, D. (1990). Effects of cholecystokinin (CCK-8) on two classes of gastroduodenal vagal afferent fibre. J. Auton. Nerv. Syst. *31*, 191–201.

Brookes, S.J., Spencer, N.J., Costa, M., and Zagorodnyuk, V.P. (2013). Extrinsic primary afferent signalling in the gut. Nat. Rev. Gastroenterol. Hepatol. *10*, 286–296.

Bucinskaite, V., Tolessa, T., Pedersen, J., Rydqvist, B., Zerihun, L., Holst, J.J., and Hellström, P.M. (2009). Receptor-mediated activation of gastric vagal afferents by glucagon-like peptide-1 in the rat. Neurogastroenterol. Motil. *21*, 978–e78.

Chambers, A.P., Sandoval, D.A., and Seeley, R.J. (2013). Integration of satiety signals by the central nervous system. Curr. Biol. *23*, R379–R388.

Chang, R.B., Strochlic, D.E., Williams, E.K., Umans, B.D., and Liberles, S.D. (2015). Vagal sensory neuron subtypes that differentially control breathing. Cell *161*, 622–633.

Fox, E.A., Phillips, R.J., Martinson, F.A., Baronowsky, E.A., and Powley, T.L. (2000). Vagal afferent innervation of smooth muscle in the stomach and duodenum of the mouse: morphology and topography. J. Comp. Neurol. *428*, 558–576.

Han, L., Ma, C., Liu, Q., Weng, H.J., Cui, Y., Tang, Z., Kim, Y., Nie, H., Qu, L., Patel, K.N., et al. (2013). A subpopulation of nociceptors specifically linked to itch. Nat. Neurosci. *16*, 174–182.

Hayes, M.R., Bradley, L., and Grill, H.J. (2009). Endogenous hindbrain glucagon-like peptide-1 receptor activation contributes to the control of food intake by mediating gastric satiation signaling. Endocrinology *150*, 2654–2659.

Hayes, M.R., De Jonghe, B.C., and Kanoski, S.E. (2010). Role of the glucagon-like-peptide-1 receptor in the control of energy balance. Physiol. Behav. *100*, 503–510.

Hillsley, K., and Grundy, D. (1998). Serotonin and cholecystokinin activate different populations of rat mesenteric vagal afferents. Neurosci. Lett. *255*, 63–66.

Holst, J.J. (2007). The physiology of glucagon-like peptide 1. Physiol. Rev. *87*, 1409–1439.

Jang, H.J., Kokrashvili, Z., Theodorakis, M.J., Carlson, O.D., Kim, B.J., Zhou, J., Kim, H.H., Xu, X., Chan, S.L., Juhaszova, M., et al. (2007). Gut-expressed gustducin and taste receptors regulate secretion of glucagon-like peptide-1. Proc. Natl. Acad. Sci. USA *104*, 15069–15074.

Jeanningros, R. (1982). Vagal unitary responses to intestinal amino acid infusions in the anesthetized cat: a putative signal for protein induced satiety. Physiol. Behav. *28*, 9–21.

Kim, Y.S., Chu, Y., Han, L., Li, M., Li, Z., Lavinka, P.C., Sun, S., Tang, Z., Park, K., Caterina, M.J., et al. (2014). Central terminal sensitization of TRPV1 by descending serotonergic facilitation modulates chronic pain. Neuron *81*, 873–887.

Lal, S., Kirkup, A.J., Brunsden, A.M., Thompson, D.G., and Grundy, D. (2001). Vagal afferent responses to fatty acids of different chain length in the rat. Am. J. Physiol. Gastrointest. Liver Physiol. *281*, G907–G915.

Lee, H., Kim, D.W., Remedios, R., Anthony, T.E., Chang, A., Madisen, L., Zeng, H., and Anderson, D.J. (2014). Scalable control of mounting and attack by Esr1+ neurons in the ventromedial hypothalamus. Nature *509*, 627–632.

Li, Y., Wu, X., Zhou, S., and Owyang, C. (2011). Low-affinity CCK-A receptors are coexpressed with leptin receptors in rat nodose ganglia: implications for leptin as a regulator of short-term satiety. Am. J. Physiol. Gastrointest. Liver Physiol. *300*, G217–G227.

Maljaars, P.W., Peters, H.P., Mela, D.J., and Masclee, A.A. (2008). Ileal brake: a sensible food target for appetite control. A review. Physiol. Behav. *95*, 271–281.

Mazda, T., Yamamoto, H., Fujimura, M., and Fujimiya, M. (2004). Gastric distension-induced release of 5-HT stimulates c-fos expression in specific brain nuclei via 5-HT3 receptors in conscious rats. Am. J. Physiol. Gastrointest. Liver Physiol. *287*, G228–G235.

Mei, N. (1978). Vagal glucoreceptors in the small intestine of the cat. J. Physiol. *282*, 485–506.

Mei, N., and Garnier, L. (1986). Osmosensitive vagal receptors in the small intestine of the cat. J. Auton. Nerv. Syst. *16*, 159–170.

Page, A.J., Slattery, J.A., Milte, C., Laker, R., O'Donnell, T., Dorian, C., Brierley, S.M., and Blackshaw, L.A. (2007). Ghrelin selectively reduces mechanosensitivity of upper gastrointestinal vagal afferents. Am. J. Physiol. Gastrointest. Liver Physiol. *292*, G1376–G1384.

Phifer, C.B., and Berthoud, H.R. (1998). Duodenal nutrient infusions differentially affect sham feeding and Fos expression in rat brain stem. Am. J. Physiol. *274*, R1725–R1733.

Powley, T.L., and Phillips, R.J. (2004). Gastric satiation is volumetric, intestinal satiation is nutritive. Physiol. Behav. *82*, 69–74.

Radu, C.G., Cheng, D., Nijagal, A., Riedinger, M., McLaughlin, J., Yang, L.V., Johnson, J., and Witte, O.N. (2006). Normal immune development and glucocorticoid-induced thymocyte apoptosis in mice deficient for the T-cell death-associated gene 8 receptor. Mol. Cell. Biol. *26*, 668–677.

Richards, W., Hillsley, K., Eastwood, C., and Grundy, D. (1996). Sensitivity of vagal mucosal afferents to cholecystokinin and its role in afferent signal transduction in the rat. J. Physiol. *497*, 473–481.

Rüttimann, E.B., Arnold, M., Hillebrand, J.J., Geary, N., and Langhans, W. (2009). Intrameal hepatic portal and intraperitoneal infusions of glucagon-like peptide-1 reduce spontaneous meal size in the rat via different mechanisms. Endocrinology *150*, 1174–1181.

Schwartz, G.J., McHugh, P.R., and Moran, T.H. (1991). Integration of vagal afferent responses to gastric loads and cholecystokinin in rats. Am. J. Physiol. *261*, R64–R69.

Sisley, S., Gutierrez-Aguilar, R., Scott, M., D'Alessio, D.A., Sandoval, D.A., and Seeley, R.J. (2014). Neuronal GLP1R mediates liraglutide's anorectic but not glucose-lowering effect. J. Clin. Invest. *124*, 2456–2463.

Thorens, B. (1992). Expression cloning of the pancreatic beta cell receptor for the gluco-incretin hormone glucagon-like peptide 1. Proc. Natl. Acad. Sci. USA *89*, 8641–8645.

Willing, A.E., and Berthoud, H.R. (1997). Gastric distension-induced c-fos expression in catecholaminergic neurons of rat dorsal vagal complex. Am. J. Physiol. *272*, R59–R67.

Wilson, D.A., and Sullivan, R.M. (2011). Cortical processing of odor objects. Neuron *72*, 506–519.

Yano, J.M., Yu, K., Donaldson, G.P., Shastri, G.G., Ann, P., Ma, L., Nagler, C.R., Ismagilov, R.F., Mazmanian, S.K., and Hsiao, E.Y. (2015). Indigenous bacteria from the gut microbiota regulate host serotonin biosynthesis. Cell *161*, 264–276.

Zagorodnyuk, V.P., Chen, B.N., and Brookes, S.J. (2001). Intraganglionic laminar endings are mechano-transduction sites of vagal tension receptors in the guinea-pig stomach. J. Physiol. *534*, 255–268.

Zhang, J., and Ritter, R.C. (2012). Circulating GLP-1 and CCK-8 reduce food intake by capsaicin-insensitive, nonvagal mechanisms. Am. J. Physiol. Regul. Integr. Comp. Physiol. *302*, R264–R273.

Zhu, J.X., Zhu, X.Y., Owyang, C., and Li, Y. (2001). Intestinal serotonin acts as a paracrine substance to mediate vagal signal transmission evoked by luminal factors in the rat. J. Physiol. *530*, 431–442.

Cell

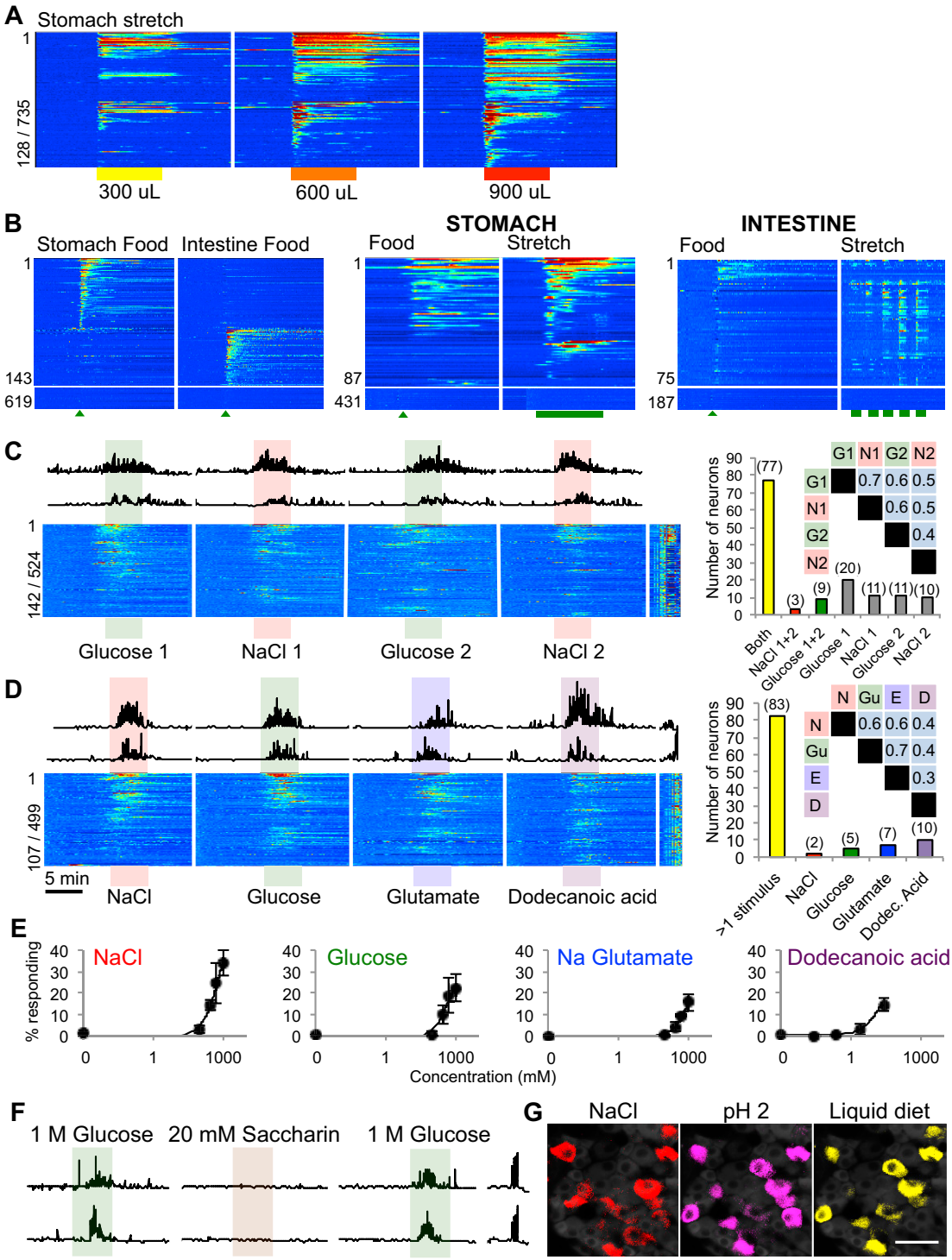

Figure S1. Imaging Ganglion Responses to Intestinal Cues, Related to Figure 1

(A) Time-resolved responses (ΔF/F, color scale) of 128 neurons (from 735 imaged) responsive to 300 μl (yellow bar, 30 s), 600 μl (orange), or 900 μl (red) volume gastric distention.

(B) Vagal ganglion imaging of sensory neuron responses to stimuli indicated. Each row indicates time-resolved GCaMP3 fluorescence intensity changes (ΔF/F, color coded) of a single neuron. Stomach stretch was achieved by inflation with nitrogen gas. Intestinal stretch was achieved by inflation with isotonic saline (green bars 30 s, 200 μl, 400 μl, 600 μl, 800 μl, 1 mL).

(legend continued on next page)

(C) Time-resolved responses following alternating perfusions of glucose (1 M in saline, green, 240 s) and sodium chloride (500 mM in saline, pink, 240 s). Top: ΔF/F of two representative neurons, bottom: ΔF/F color scale of 142 responsive neurons (out of 524 viable imaged neurons). Graph (right) indicates the number of neurons responsive to both glucose and sodium chloride (yellow), or either stimulus alone. Correlation coefficients of response patterns across the neuron repertoire were calculated for each stimulus pair (G1- glucose 1; N1- sodium chloride 1; G2- glucose 2; N2- sodium chloride 2).
(D) Time-resolved responses (top: ΔF/F of two representative neurons, bottom: ΔF/F color scale of 107 responsive neurons, from 499 imaged) following perfusion of stimuli indicated. Graph (right) indicates numbers of neurons responsive to multiple luminal cues (yellow), or to single cues. Correlation coefficients of response patterns across the neuron repertoire were calculated for each stimulus pair (N- sodium chloride 1; Gu- glucose; E- glutamate; D- dodecanoic acid).
(E) Percentage of neurons responsive to intestinal stimuli at different concentrations. (n = 3 mice per stimulus, ± sem).
(F) Time-resolved responses (ΔF/F) of two representative neurons to intestinal perfusion (240 s) of the artificial sweetener saccharin (20 mM) and glucose (1 M).
(G) GCaMP3 fluorescence changes in vagal ganglia following introduction of salt (red), low pH (magenta), and liquid diet (yellow) into the duodenal bulb. Scale bar, 50 μm.

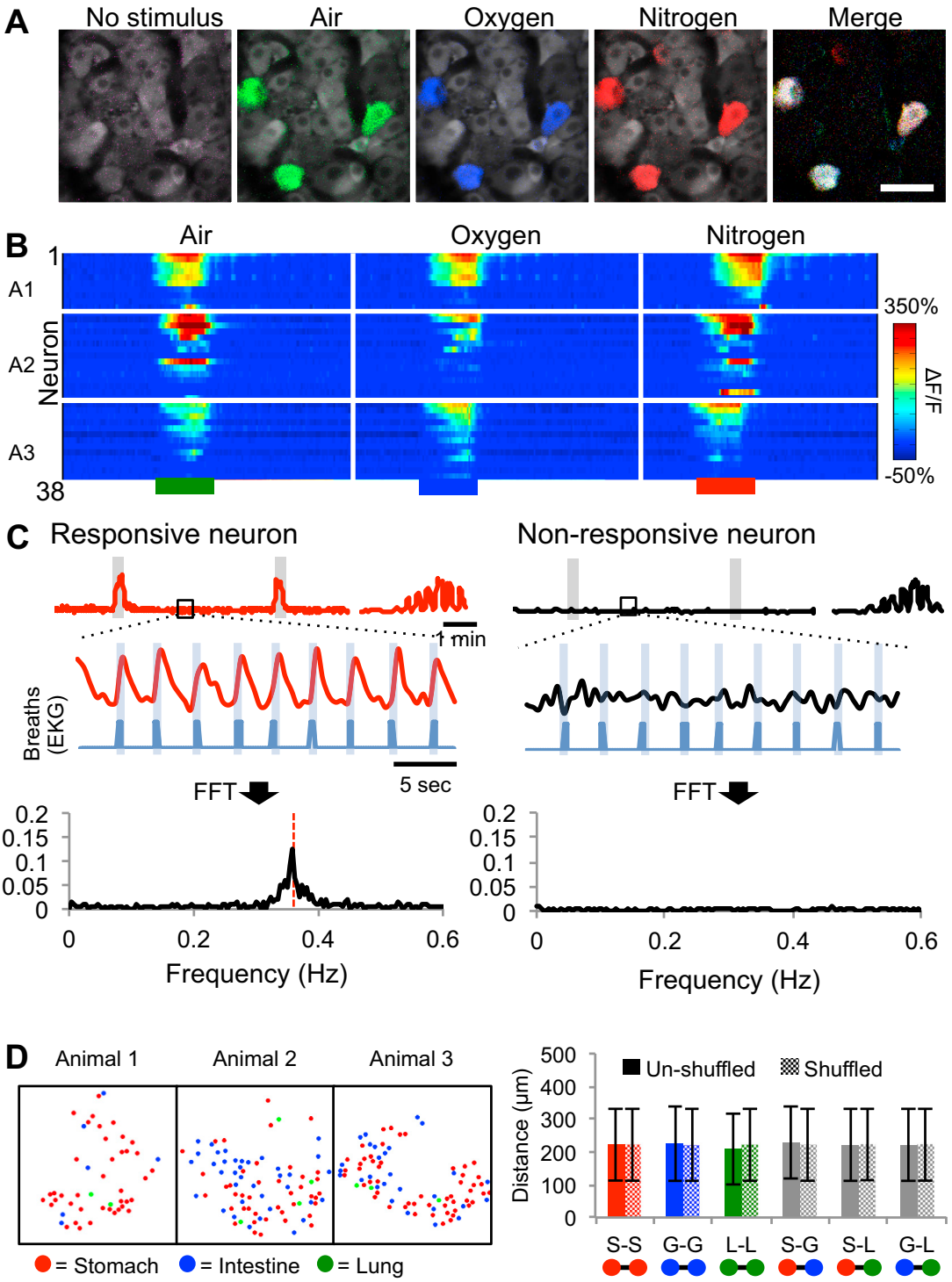

Figure S2. Lung Mechanoreceptors Are Entrained to Tidal Breathing; Salt and Pepper Organization of Vagal Inputs, Related to Figure 1

(A) Single neuron responses before (no stimulus) and during lung inflation with ambient air (green), oxygen (blue), and nitrogen (red) visualized by confocal microscopy of vagal ganglia.

(B) Time-resolved responses (ΔF/F, color scale) of all 38 responsive neurons (3 mice, A1-3) to lung inflation (30 s, colored bars) by stimuli indicated.

(C) Representative responses during tidal breathing of single neurons that detect (responsive neuron) or do not detect (non-responsive neuron) lung stretch (gray bars). Neuron viability was verified by electrical stimulation (right). Breaths observed by electrocardiogram recordings (blue bars) are aligned with activity traces (black, red) in figure inset. Bottom: Fast-fourier transformation (FFT) analysis was used to derive neuron oscillation frequencies.

(legend continued on next page)

(D) Position in the imaging field of neurons responsive to stomach stretch (red), intestinal glucose (blue) and lung inflation (green). Average distance between two neurons responsive to stimuli indicated (S- stomach stretch; G- intestinal glucose; L- lung inflation). Calculations were repeated with the same dataset in which neuron response properties were randomly assigned ('shuffled') and no differences were observed. (n = 245 neurons from 4 mice, ± sd).

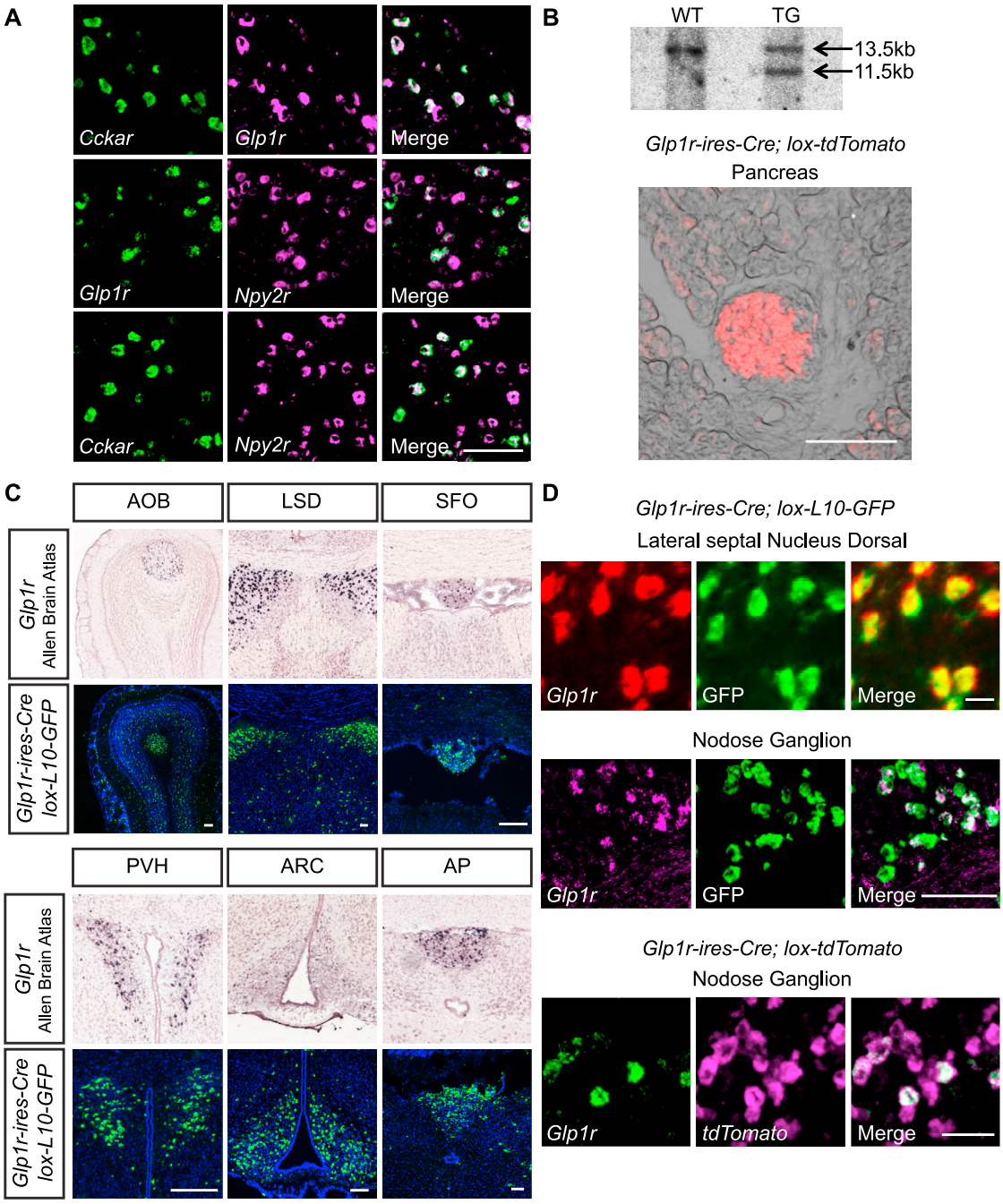

Figure S3. Characterization of Vagal GLP1R Neurons and *Glp1-ires-Cre* Knockin Mice, Related to Figure 2

(A) Two color FISH in vagal ganglion cryosections reveals frequent co-expression of CCKAR, GLP1R, and NPY2R. NPY2R marks a larger neuron cohort suggesting two principal neuron subtypes: NPY2R^{+}/CCKAR^{+}/GLP1R^{+} and NPY2R^{+}/CCKAR^{-}/GLP1R^{-}. Scale bar, 100 μm.

(B) Top: Southern Blot analysis of genomic DNA from wild-type (WT) and *Glp1r-ires-Cre* heterozygous mice (TG). Bottom: native tdTomato fluorescence in pancreas of *Glp1r-ires-Cre; lox-tdTomato* mice. Scale bar, 100 μm.

(C) Cell types (AOB: accessory olfactory bulb, LSD: lateral septal nucleus dorsal; SFO: subfornical organ; PVH: paraventricular nucleus; ARC: arcuate nucleus; AP: area postrema) that express *Glp1r*. Top: *Glp1r in situ* hybridization from Allen Brain Atlas (Lein et al., 2007) and bottom: GFP expression in *Glp1r-ires-Cre; lox-L10-GFP* mice (GFP immunofluorescence in tissue cryosections); scale bar, 100 μm.

(D) Top, middle; FISH for *Glp1r* (red/magenta) superimposed on native GFP fluorescence in *Glp1r-ires-Cre; lox-L10-GFP* mice. Bottom: two-color FISH for *Glp1r* and *tdTomato* in *Glp1r-ires-Cre; lox-tdTomato* mice. Scale bars, 20 μm (top), 100 μm (middle), 50 μm (bottom).

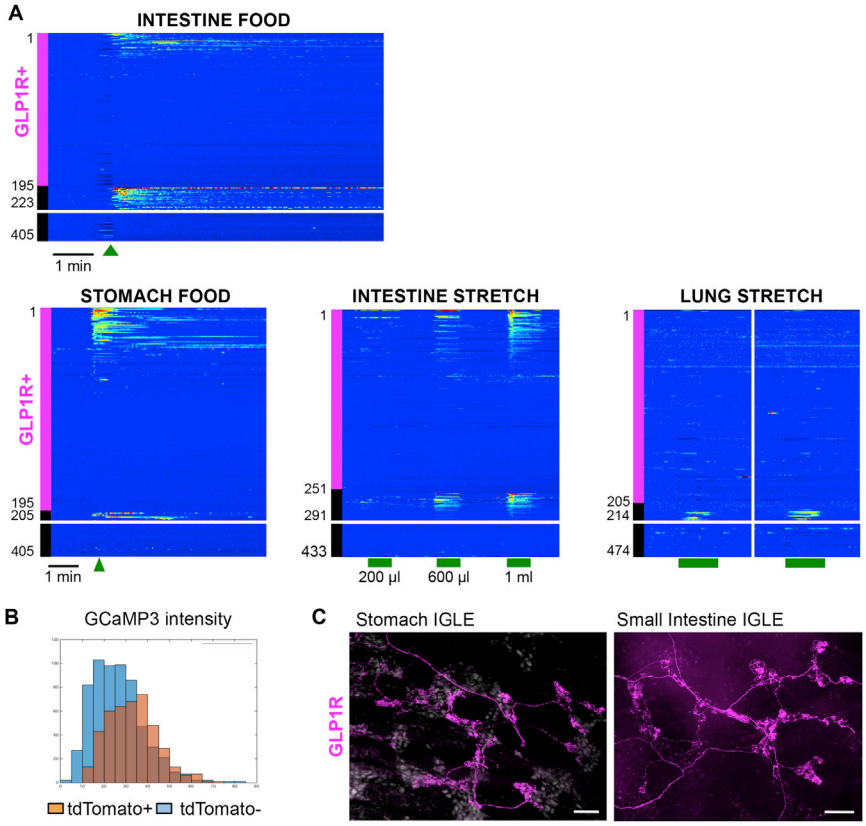

Figure S4. In Vivo Responses and Anatomy of Vagal GLP1R Neurons, Related to Figure 2

(A) Time-resolved GCaMP3 fluorescence intensity changes (ΔF/F, color coded) of single vagal neurons in ganglion of *Glp1r-GCaMP3** mice to stimuli indicated (intestine stretch: 30 s; lung stretch: 15 s). tdTomato-positive and tdTomato-negative neurons are distinguished on the left (magenta and black bars respectively). Only some unresponsive tdTomato-negative neurons are depicted; numbers at y axis base indicate total number of viable imaged neurons.

(B) Histogram of baseline GCaMP3 fluorescence in tdTomato^{+} (orange) and tdTomato^{-} (blue) neurons.

(C) GLP1R neurons, visualized by AAV mapping in *Glp1r-ires-Cre* mice, form IGLE terminals in stomach and intestine. Enteric neurons were counterstained with Fluorogold (gray). Scale bar, 100 µm.

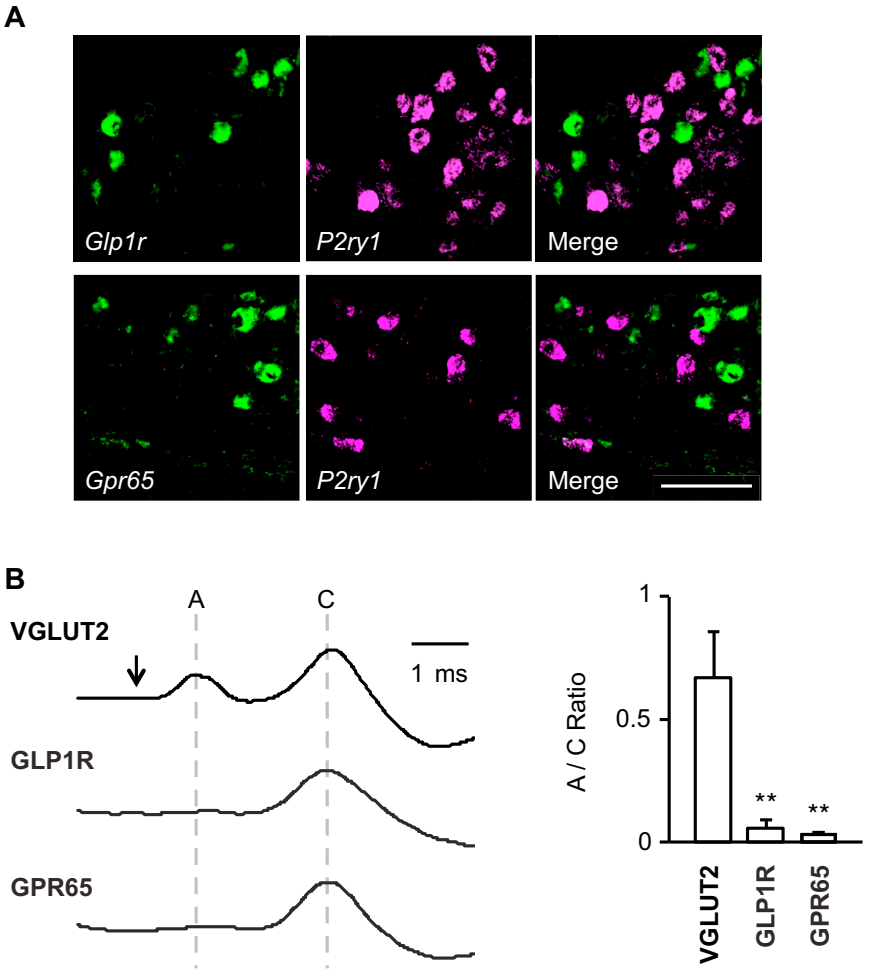

Figure S5. Characterization of Vagal Afferent Subtypes, Related to Figures 3 and 4

(A) GLP1R and GPR65 neurons do not contain P2RY1. Two-color FISH in vagal ganglia using cRNA riboprobes for *Glp1r* (green, top), *Gpr65* (green, bottom), and *P2ry1* (magenta) reveals predominant expression in different sensory neurons. Scale bar, 100 μm.

(B) Compound action potentials after brief optogenetic stimulation (arrow) in *Vglut2-ChR2*, *Glp1r-ChR2*, and *Gpr65-ChR2* mice show A and C fibers (mean ± sem, n = 4-5, $^{**}p < 0.01$).

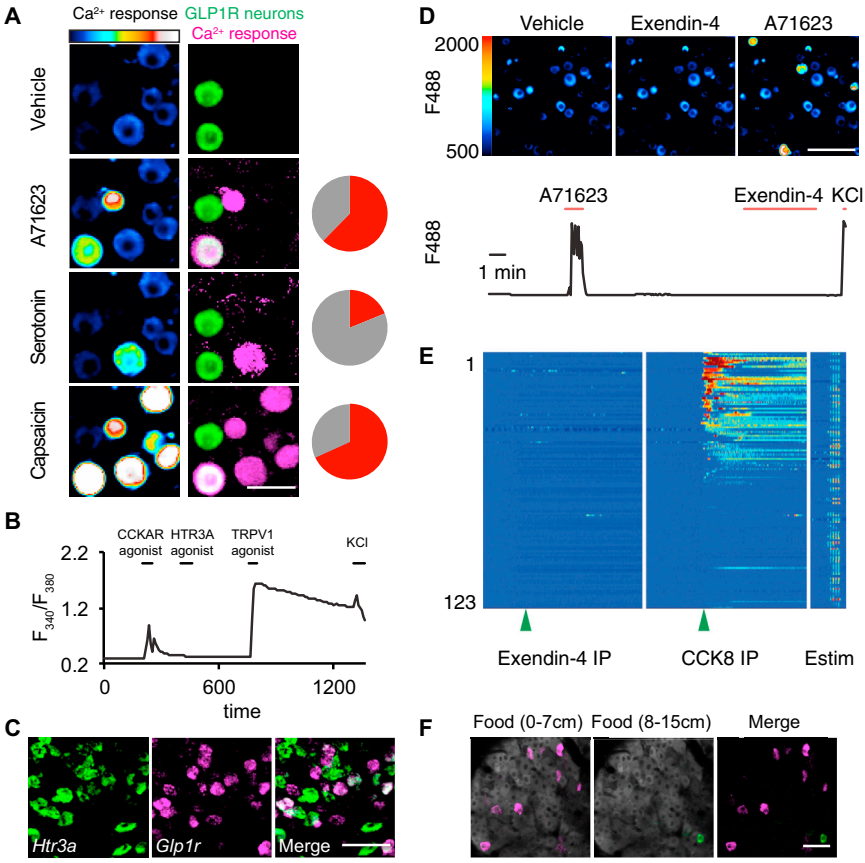

Figure S6. Hormone and Nutrient Responses in Vagal Afferent Types, Related to Figures 5 and 6

(A) Calcium responses by Fura-2 imaging of dissociated vagal sensory neurons from *Glp1r-ires-Cre; lox-L10-GFP* mice to the CCKAR agonist A71623 (100 nM), serotonin (10 μM), and capsaicin (2 μM). Scale bar, 40 μm. Left: Fura-2 excitation; middle: GFP fluorescence (green) and calcium responses (magenta), right: pie chart indicating percentage of GLP1R neurons activated (red) by each ligand.

(B) Representative responses of a GLP1R neuron.

(C) Two color FISH in vagal ganglia using riboprobes for *Htr3a* (green) and *Glp1r* (magenta). Scale bar, 100 μm.

(D) The GLP1R agonist exendin-4 does not acutely activate vagal sensory neurons in vitro. Calcium responses to agonists for GLP1R (exendin-4, 100 nM) and CCKAR (A71623, 100 nM) were imaged using GCaMP3 in dissociated vagal sensory neurons from *Vglut2-ires-Cre*; *lox-GCaMP3* mice. Top: GCaMP3 fluorescence (color scale) visualized by microscopy. Scale bar, 100 μm; bottom: responses of a single neuron.

(E) In vivo ganglion imaging reveals that the GLP1R agonist exendin-4 does not acutely activate vagal sensory neurons in vivo. Responses in 123 electrical stimulation-activated neurons (E-stim) were measured in response to intraperitoneal (IP) injection of exendin-4 (10 μM) and CCK8 (100 μM).

(F) In vivo ganglion imaging during food injection in the proximal (0-7 cm) and distal (8-15 cm) intestine.

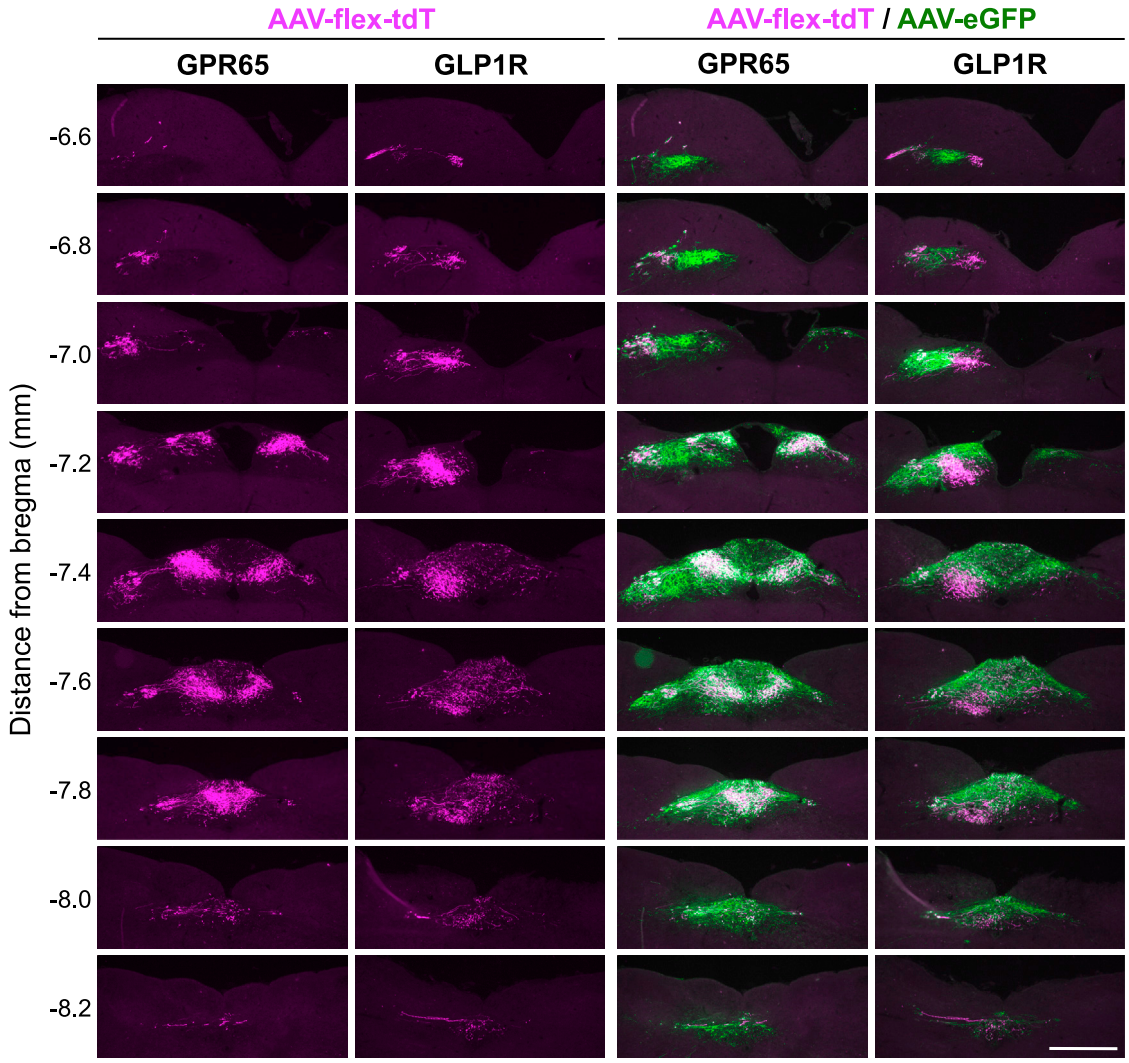

Figure S7. Brainstem Projections of Vagal GLP1R and GPR65 Neurons Are Revealed along the Entire Anterior-Posterior Axis, Related to Figure 7

Vagal ganglia of *Gpr65-ires-Cre* and *Glp1-ires-Cre* mice were infected with *AAV-flex-tdTomato* and *AAV-GFP*, and axons visualized in the brainstem by two-color immunofluorescence. A dorsomedial region of each coronal section is depicted, similar to Figure 7A. Scale bar, 500 μm.

Cell, Volume *166*

Supplemental Information

Sensory Neurons that Detect Stretch and Nutrients in the Digestive System

Erika K. Williams, Rui B. Chang, David E. Strochlic, Benjamin D. Umans, Bradford B. Lowell, and Stephen D. Liberles

SUPPLEMENTAL EXPERIMENTAL PROCEDURES

Animals

All animal procedures complied with institutional animal care and use committee guidelines. *Glp1r-ires-Cre* mice were prepared using standard BAC recombineering approaches (Chang et al., 2015). *Glp1r* and *Gpr65* Southern blots involved genomic DNA cut with SphI and BamHI respectively and probes generated by PCR using specific primers (*Glp1r*: GGGTGTGGAGAGGACCTGGTCACTGTG and AATACATGGCCACTCACAGAGCCACCC; *Gpr65*: CAGTTTGCATGTGAACCTGC and CTCACTTTCTGCTTTATCCC). PCR primers used for genotyping *Glp1r-ires-Cre* mice were GTTTCTTCCTCTCTTCCTGCC and either TCATCAAGCCCATCTCTCTCC (wild type) or ACCGCTTCCTCGTGCTTTAC (knock-in). *Gpr65-ires-Cre*, *P2ry1-ires-Cre*, *Vglut2-ires-Cre*, and *lox-L10-GFP* mice were described previously (Chang et al., 2015; Krashes et al., 2014; Vong et al., 2011; Zhou et al., 2010). *lox-GCaMP3* (014538), *lox-tdTomato* (007908), *lox-ChR2* (012569) and $Gpr65^{GFP/+}$ (008577) lines were purchased (Jackson). The constitutive *GCaMP3* allele (*Rosa26-GCaMP3*) was generated by breeding *lox-GCaMP3* with *E2a-Cre* mice (Jackson, 003314), and then crossing out the *E2a-Cre* allele. Experimental groups were assigned based on genotypes, and were randomized with respect to animal gender and age (> 5 weeks old).

RNA *in situ* hybridization

In situ hybridization studies were performed on 10-20 μm cryosections of vagal ganglia as described (Chang et al., 2015). cRNA riboprobes were prepared for *Glp1r* (1392 bp amplified with primers ATGGCCAGCACCCCAAGC and TCAGCTGTAGGAACTCTGG), *Htr3a* (845 bp amplified by primers CAACGGCCATCGGTACCCCC and ATGAGCAGTTCCAGGGGCCG), and *Cckar* (994 bp amplified with primers AGGAGGAAGATGGAAGGACC and GCTACTTATTAAGTGAGTCCC). Other riboprobes were described previously (Chang et al., 2015).

In vitro calcium imaging

Fura-2 based calcium imaging in acutely dissociated vagal sensory neurons was performed as described (Chang et al., 2015) using *Glp1r-ires-Cre; lox-L10-GFP* and $Gpr65^{GFP/+}$ mice. Test chemicals were dissolved in Hank's balanced salt solution and included CCKAR agonist A71623 (100 nM, Tocris), CCK-8 (10 nM, Sigma), Exendin-4 (100 nM, Tocris), serotonin (10 μM, Sigma), *m*-chlorophenylbiguanide (100 μM, Sigma), and capsaicin (1-2 μM, Sigma). Only cells that responded to KCl (50 mM) were counted. GCaMP3 imaging involved *Vglut2-ires-Cre; lox-GCamp3* mice, and were imaged with excitation-emission filters for GFP.

AAV-guided anatomical mapping

AAVs were introduced into vagal ganglia of adult (2-4 months old) *Gpr65-ires-Cre* and *Glp1r-ires-Cre* mice as described (Chang et al., 2015). Enteric neurons were labeled by intraperitoneal injection of Fluorogold (30 mg/kg) (Powley and Berthoud, 1991). Innervation of duodenum was quantified in cryosections (12 μm) sampled every millimeter from the pyloric sphincter over a distance of 1 centimeter. For whole mount analysis of IGLE innervation, the ventral stomach corpus was dissected and the muscular layer gently isolated. Immunohistochemistry for tdTomato and GFP was performed using techniques and antibodies described (Chang et al., 2015), and intestinal cryosections were counterstained with 4',6-diamidino-2-phenylindole (DAPI). Normalized villus innervation was quantified by dividing the number of villi innervated with tdTomato-containing fibers by the number of villi innervated with GFP-containing fibers. Stomach IGLEs were identified using standard criteria (Wang and Powley, 2000), and the numbers of enteric ganglia innervated were counted. Some animals with low AAV infection rates (<10% of neurons) were excluded based on analysis of GFP fluorescence in vagal ganglia; exclusions were determined blind to animal genotype and prior to analysis of peripheral and central innervation. In Figures 2 and 4, DAPI and Fluorogold fluorescence images were gamma-corrected to enhance visualization of tissue architecture and Sobel edge detection was used to enhance display of tdTomato fibers in low magnification images. Non-linear enhancements were not used prior to quantification. Experimenters were blinded to animal genotype for quantification.

Optogenetics and physiology

Studies involving optogenetics, whole nerve electrophysiology to quantify neuron conduction velocity, and physiological measurements of heart rate, gastric pressure, and respiratory rate were as described (Chang et al., 2015). Gastric contractions were not measured in two animals (both *lox-ChR2*) prior to optogenetic stimulation and were excluded from analysis.

In vivo imaging

Mice (24 hour fasted) were placed under continuous anesthesia (isofluorane/oxygen), and kept at normal body temperature. The ventral neck surface was shaved and cleaned, and a one-inch midline incision was made above the sternum and below the jaw. The trachea was exposed by separating the submandibular and sublingual glands, and the left glands were excised with residual tissue cauterized to prevent bleeding. The sternocleidomastoid muscle and associated soft tissue was moved laterally using a magnetic retractor, exposing the common carotid artery, internal jugular vein, and vagus nerve trunk. The vagus nerve trunk, inclusive of the superior laryngeal branch, was gently separated from the carotid artery and surrounding soft tissue, and a second magnetic retractor was used to pull the carotid artery and trachea medially. The hypoglossal nerve was transected, and a third magnetic retractor was used to displace small carotid artery branches close to the jugular foramen. Vagus nerve transections were made superior to the jugular ganglion and at the auricular and meningeal branches to free the ganglion so it could be placed on a stable imaging platform: a 5 mm diameter glass coverslip (NeuVitro GG-5-0) glued to a custom metal arm affixed to a micromanipulator (WPI, M3301L) for high precision control of the imaging field. Magnetic retractors were removed. The ganglion was embedded in KwikSil adhesive (WPI), and a second coverslip placed on top and allowed to set (15 minutes). A water-tight wall was constructed around the entire surgical site using silicone, and the neck cavity containing the immobilized ganglion was immersed in Lactated Ringer's solution into which the microscope objective was lowered. Imaging was performed with an upright confocal microscope (Leica TCS SP5 II) using a 20x, NA1.00 water-immersion objective (5 μm optical thickness, < 90 μW laser power to prevent tissue damage, 2 Hz frame rate). Stimuli were introduced (see below), and heart rate and respiration were measured by EKG. GCaMP3 fluorescence changes were obtained (Fiji with Time Series Analyzer V 2.0 plug-in) in regions of interest (ROIs), with each ROI confined to a single cell throughout the entire imaging session. ROI intensities (average across pixels) were calculated in each frame and exported to MatLab for analysis. Responses were also manually analyzed, and rarely, responses were excluded if baseline fluorescence shifted during the experiment, for example from a movement artifact.

Electrical stimulation of the cervical vagus nerve occurred in steps (10 seconds of 2 millisecond pulses at 5 Hz, Grass S5 Stimulator) of increasing voltage (stepwise from 1 to 70 V). Gases were introduced into the airways via a tracheal cannula (flow rate: 1 liter/minute). Tubing (PE-10, Braintree Scientific) was passed through a needle-sized hole (18 gauge) in the trachea wall between the first and second cartilaginous segments, and advanced to the carina. Gastric distension was achieved by inflation of a surgically implanted latex balloon (Braintree Scientific, 73-3478) affixed to a small rodent feeding needle (FST, 18061-20) and syringe, which allowed for precise volume control by manual infusion of liquid. After removal of stomach contents through an incision in the greater curvature of the stomach, the balloon was surgically implanted near the gastroduodenal sphincter, and the incision site sealed with Vetbond tissue glue. Gastric distension was also achieved by inflating the stomach with nitrogen gas (3-6 ml/min, 15 seconds) after surgical closure of the pyloric sphincter. For single-bolus nutrient introductions (Figures 1E, 2, 6, S1B, S4, S6), the gastro-duodenal sphincter was first sealed by tightening a surgical thread circumferentially. Liquid diet (200 μl, TestDiet 0054451, 37°C) was then introduced into the stomach and small intestine with a small (26 gauge) needle. For intestinal perfusions (Figures 1C, 1D, 1F, S1C-F), a small rodent feeding needle was inserted through an incision in the stomach, pushed past the gastroduodenal sphincter, and placed in the proximal duodenum within 0.5 centimeters of the sphincter, which was sealed with tissue adhesive. The intestine was transected ~11 centimeters distally to create an exit port, and saline (HBSS, Gibco 14025-126) was continuously perfused (125 μl/minute) using a peristaltic pump, with stimuli periodically introduced (240 seconds). Prior to intestinal stretch, intestinal contents were flushed with saline, and stretch was introduced by introducing fixed liquid volumes in the presence of an exit port clamp. Experiments were excluded if surgical complications prevented stimulus delivery or imaging.

Baseline signal was defined as the average GCaMP3 fluorescence over a 3 minute period prior to stimulus introduction. Neurons were only included in analysis if they responded to electrical stimulation at the end of an experimental session (with maximal GCaMP3 fluorescence > seven standard deviations above baseline mean), and did not drift out of the imaging field. Cells were coded as responsive to liquid diet if both of two criteria were met: 1) peak GCaMP3 fluorescence was two standard deviations above the baseline mean within 250 seconds of stimulus introduction and 2) the mean GCaMP3 fluorescence over a 20 second window around the peak response was >50% above baseline. Cells were coded as responsive to mechanical stimuli (lung, stomach, intestine) if either of two criteria were met: 1) maximal GCaMP3 fluorescence was > seven standard deviations above the baseline mean during the stimulus (for rapidly adapting responses) or 2) if mean GCaMP3 fluorescence was > three standard deviations above baseline mean during the entire stimulus (for slowly adapting responses). Neurons displaying oscillatory behavior were identified by fast-fourier transformation of baseline activity, with peaks defined between 0.1 and 0.75 Hz and > 5 standard deviations above mean baseline fluctuations (Figure S2). Correlation coefficients

(Figure S1) were derived from stimulus pairs across the neuron repertoire by comparing response amplitudes for each neuron (mean ΔF/F in a 2 minute window around signal peak). During imaging in *Glp1r-GCaMP3** and *Gpr65-GCaMP3** mice, GCaMP3 fluorescence data was collected using a narrow bandwidth of 500-540 nm, which resulted in similar baseline GCAMP3 fluorescence measurements between tdTomato-positive and tdTomato-negative neurons (Figure S4). Neuron positions were defined using Cartesian coordinates, with position standardization to allow for comparisons between ganglia. Experimenters were blinded to neuron identity (defined by tdTomato expression) or prior neuron responsiveness during imaging analysis.

Code availability
Imaging data was analyzed using the publicly available software package, Fiji (http://fiji.sc/Fiji), using the Time Series Analyzer plugin (http://rsb.info.nih.gov/ij/plugins/time-series.html). Matlab scripts to convert imaging signals to ΔF/F, categorize responsive vs non-responsive neurons, and generate raster plots were written in the laboratory, and are available upon request.

Data analysis
Sample sizes are indicated in main text, figure legends, or bar graphs (numbers in parentheses). Significance was determined by comparisons to the indicated control group using a two-tailed Student's t test (Fig. 2, 3) or between indicated groups using a two-tailed Mann-Whitney test (Fig. 4). For optogenetics and physiological studies, data were normally distributed, and compared groups had similar variance. All experiments involved biological rather than technical replicates.

SUPPLEMENTAL REFERENCES

Krashes, M.J., Shah, B.P., Madara, J.C., Olson, D.P., Strochlic, D.E., Garfield, A.S., Vong, L., Pei, H., Watabe-Uchida, M., Uchida, N.*, et al.* (2014). An excitatory paraventricular nucleus to AgRP neuron circuit that drives hunger. Nature *507*, 238-242.

Lein, E.S., Hawrylycz, M.J., Ao, N., Ayres, M., Bensinger, A., Bernard, A., Boe, A.F., Boguski, M.S., Brockway, K.S., Byrnes, E.J.*, et al.* (2007). Genome-wide atlas of gene expression in the adult mouse brain. Nature *445*, 168-176.

Powley, T.L., and Berthoud, H.R. (1991). A fluorescent labeling strategy for staining the enteric nervous system. J Neurosci Methods *36*, 9-15.

Vong, L., Ye, C., Yang, Z., Choi, B., Chua, S., Jr., and Lowell, B.B. (2011). Leptin action on GABAergic neurons prevents obesity and reduces inhibitory tone to POMC neurons. Neuron *71*, 142-154.

Wang, F.B., and Powley, T.L. (2000). Topographic inventories of vagal afferents in gastrointestinal muscle. J Comp Neurol *421*, 302-324.

Zhou, X., Wang, L., Hasegawa, H., Amin, P., Han, B.X., Kaneko, S., He, Y., and Wang, F. (2010). Deletion of PIK3C3/Vps34 in sensory neurons causes rapid neurodegeneration by disrupting the endosomal but not the autophagic pathway. Proceedings of the National Academy of Sciences of the United States of America *107*, 9424-9429.

SUPPLEMENTAL FIGURE LEGENDS

Figure S1: Imaging ganglion responses to intestinal cues, Related to Figure 1.
(A) Time-resolved responses (ΔF/F, color scale) of 128 neurons (from 735 imaged) responsive to 300 µl (yellow bar, 30 seconds), 600 µl (orange), or 900 µl (red) volume gastric distention. (B) Vagal ganglion imaging of sensory neuron responses to stimuli indicated. Each row indicates time-resolved GCaMP3 fluorescence intensity changes (ΔF/F, color coded) of a single neuron. (C) Time-resolved responses following alternating perfusions of glucose (1 M in saline, green, 240 seconds) and sodium chloride (500 mM in saline, pink, 240 seconds). Top: ΔF/F of two representative neurons, bottom: ΔF/F color scale of 142 responsive neurons (out of 524 viable imaged neurons). Graph (right) indicates the number of neurons responsive to both glucose and sodium chloride (yellow), or either stimulus alone. Correlation coefficients of response patterns across the neuron repertoire were calculated for each stimulus pair (G1- glucose 1; N1- sodium chloride 1; G2- glucose 2; N2- sodium chloride 2). (D) Time-resolved responses (top: ΔF/F of two representative neurons, bottom: ΔF/F color scale of 107 responsive neurons, from 499 imaged) following perfusion of stimuli indicated. Graph (right) indicates numbers of neurons responsive to multiple luminal cues (yellow), or to single cues. Correlation coefficients of response patterns across the neuron repertoire were calculated for each stimulus pair (N- sodium chloride 1; Gu- glucose; E- glutamate; D- dodecanoic acid). (E) Percentage of neurons responsive to intestinal stimuli at different concentrations. (n = 3 mice per stimulus, ± sem). (F) Time-resolved responses (ΔF/F) of two representative neurons to intestinal perfusion (240 seconds) of the artificial sweetener saccharin (20 mM) and glucose (1 M). (G) GCaMP3 fluorescence changes in vagal ganglia following introduction of salt (red), low pH (magenta), and liquid diet (yellow) into the duodenal bulb, scale bar: 50 µm.

Figure S2: Lung mechanoreceptors are entrained to tidal breathing; salt and pepper organization of vagal inputs, Related to Figure 1.
(A) Single neuron responses before (no stimulus) and during lung inflation with ambient air (green), oxygen (blue), and nitrogen (red) visualized by confocal microscopy of vagal ganglia. (B) Time-resolved responses (ΔF/F, color scale) of all 38 responsive neurons (3 mice) to lung inflation (30 seconds, colored bars) by stimuli indicated. (C) Representative responses during tidal breathing of single neurons that detect (responsive neuron) or do not detect (non-responsive neuron) lung stretch (grey bars). Neuron viability was verified by electrical stimulation (right). Breaths observed by electrocardiogram recordings (blue bars) are aligned with activity traces (black, red) in figure inset. Bottom: Fast-fourier transformation (FFT) analysis was used to derive oscillation frequencies. (D) Position in the imaging field of neurons responsive to stomach stretch (red), intestinal glucose (blue) and lung inflation (green). Average distance between two neurons responsive to stimuli indicated (S- stomach stretch; G- intestinal glucose; L- lung inflation). Calculations were repeated with the same data set in which neuron response properties were randomly assigned ('shuffled') and no differences were observed. (n= 245 neurons from 4 mice, ± sd).

Figure S3. Characterization of vagal GLP1R neurons and *Glp1-ires-Cre* knock-in mice, Related to Figure 2.
(A) Two color FISH in vagal ganglion cryosections reveals frequent co-expression of CCKAR, GLP1R, and NPY2R. NPY2R marks a larger neuron cohort suggesting two principal neuron subtypes: $NPY2R^{+}/CCKAR^{+}/GLP1R^{+}$ and $NPY2R^{+}/CCKAR^{-}/GLP1R^{-}$. (B) Top: Southern Blot analysis of genomic DNA from wild type (WT) and *Glp1r-ires-Cre* heterozygous mice (TG). Bottom: native tdTomato fluorescence in pancreas of *Glp1r-ires-Cre; lox-tdTomato* mice, scale bar: 100 µm. (C) Cell types (AOB: accessory olfactory bulb, LSD: lateral septal nucleus dorsal; SFO: subfornical organ; PVH: paraventricular nucleus; ARC: arcuate nucleus; AP: area postrema) that express *Glp1r*. Top: *Glp1r in situ* hybridization from Allen Brain Atlas (Lein et al., 2007) and bottom: GFP expression in *Glp1r-ires-Cre; lox-L10-GFP* mice (GFP immunofluorescence in tissue cryosections), scale bar: 100 µm. (D) Top, middle; FISH for *Glp1r* (red/magenta) superimposed on native GFP fluorescence in *Glp1r-ires-Cre; lox-L10-GFP* mice. Bottom: two-color FISH for *Glp1r* and *tdTomato* in *Glp1r-ires-Cre; lox-tdTomato* mice. Scale bars: 20 µm (top), 100 µm (middle), 50 µm (bottom).

Figure S4: *In vivo* responses and anatomy of vagal GLP1R neurons, Related to Figure 2.
(A) Time-resolved GCaMP3 fluorescence intensity changes (ΔF/F, color coded) of single vagal neurons in ganglion of *Glp1r-GCaMP3** mice to stimuli indicated (intestine stretch: 30 seconds; lung stretch: 15 seconds). tdTomato-positive and tdTomato-negative neurons are distinguished on the left (magenta and black bars respectively). Only some unresponsive tdTomato-negative neurons are depicted; numbers at Y axis base indicate total number of viable imaged neurons. (B) Histogram of baseline GCaMP3 fluorescence in $tdTomato^{+}$ (orange) and $tdTomato^{-}$ (blue)

neurons. (C) GLP1R neurons, visualized by AAV mapping in *Glp1r-ires-Cre* mice, form IGLE terminals in stomach and intestine. Enteric neurons were counterstained with Fluorogold (grey). Scale bar: 100 μm.

Figure S5. Characterization of vagal afferent subtypes, Related to Figures 3 and 4.
(A) GLP1R and GPR65 neurons do not contain P2RY1. Two-color FISH in vagal ganglia using cRNA riboprobes for *Glp1r* (green, top), *Gpr65* (green, bottom), and *P2ry1* (magenta) reveals predominant expression in different sensory neurons, scale bar: 100 μm. (B) Compound action potentials after brief optogenetic stimulation (arrow) in *Vglut2-ChR2*, *Glp1r-ChR2*, and *Gpr65-ChR2* mice show A and C fibers (mean ± sem, n=4-5, **p<.01).

Figure S6. Hormone and nutrient responses in vagal afferent types, Related to Figures 5 and 6.
(A) Calcium responses by Fura-2 imaging of dissociated vagal sensory neurons from *Glp1r-ires-Cre; lox-L10-GFP* mice to the CCKAR agonist A71623 (100 nM), serotonin (10 μM), and capsaicin (2 μM), scale bar: 40 μm. Left: Fura-2 excitation; middle: GFP fluorescence (green) and calcium responses (magenta), right: pie chart indicating percentage of GLP1R neurons activated (red) by each ligand. (B) Representative responses of a GLP1R neuron. (C) Two color FISH in vagal ganglia using riboprobes for *Htr3a* (green) and *Glp1r* (magenta), scale bar: 100 μm. (D) The GLP1R agonist exendin-4 does not acutely activate vagal sensory neurons *in vitro*.
Calcium responses to agonists for GLP1R (exendin-4, 100 nM) and CCKAR (A71623, 100 nM) were imaged using GCaMP3 in dissociated vagal sensory neurons from *Vglut2-ires-Cre*; *lox-GCaMP3* mice. Top: GCaMP3 fluorescence (color scale) visualized by microscopy, scale bar: 100 μm; bottom: responses of a single neuron. (E) *In vivo* ganglion imaging reveals that the GLP1R agonist exendin-4 does not acutely activate vagal sensory neurons *in vivo*. Responses in 123 electrical stimulation-activated neurons (E-stim) were measured in response to intraperitoneal (IP) injection of exendin-4 (10 μM) and CCK8 (100 μM). (F) *In vivo* ganglion imaging during food perfusion through the proximal (0-7 cm) and distal (8-15 cm) intestine.

Figure S7. Brainstem projections of vagal GLP1R and GPR65 neurons are revealed along the entire anterior-posterior axis, Related to Figure 7.
Vagal ganglia of *Gpr65-ires-Cre* and *Glp1-ires-Cre* mice were infected with *AAV-flex-tdTomato* and *AAV-GFP*, and axons visualized in the brainstem by two-color immunofluorescence. A dorsomedial region of each coronal section is depicted, similar to Figure 7A, scale bar: 500 μm.

Supplementary Video. Imaging of vagal ganglia reveals single neuron responses to nerve trunk electrical stimulation
GCaMP3 fluorescence in vagal ganglia of *Vglut2-ires-Cre; lox-GCaMP3* mice was imaged by confocal microscopy. Voltage pulses were applied to the vagus nerve trunk, evoking repeated calcium transients visualized by changes in GCaMP3 fluorescence intensity.